American Mineralogist, Volume 92, pages 1165–1180, 2007

Cation ordering in $MgTi_2O_5$ (karrooite): Probing temperature dependent effects with neutrons

Alistair R. Lennie,[1,*] Kevin S. Knight,[2] and C. Michael B. Henderson[1,3]

[1]CCLRC Daresbury Laboratory, Keckwick Lane, Warrington, Cheshire, WA4 4AD, U.K.
[2]ISIS, CCLRC Rutherford Appleton Laboratory, Chilton, Oxfordshire, OX11 0QX, U.K.
[3]School of Earth, Atmospheric and Environmental Sciences, University of Manchester, Oxford Road, Manchester, M13 9PL, U.K.

Abstract

$MgTi_2O_5$ (karrooite) exhibits cation exchange between the two non-equivalent octahedral M1 and M2 sites. The temperature dependence of Ti-Mg disorder has been determined using in situ time-of-flight powder neutron diffraction to establish the cation population of each site. The equilibrium Ti-Mg exchange commences above 700–800 °C, and continues up to 1300 °C. At ~1350 °C $MgTi_2O_5$ appears to undergo a reversible, displacive phase transition, although the structure can still be refined in space group 63. This transition shows discontinuities in the degree of order, the *c* cell parameter, and in the M-O bond lengths, quadratic elongation, and bond angle variance for the M1 octahedron, which becomes pseudo-tetrahedral. By contrast, the M2 octahedron shows no significant change. An Arrhenius plot exhibits linear behavior from 750–1300 °C, gives an exchange enthalpy of ordering of 33.6 kJ/mol, and a value of 10.7 kJ/mol for the entropy of disordering. A value of 5.92 cm^3/mol is deduced for the ΔV of the high-temperature reaction of geikielite ($MgTiO_3$) + rutile (TiO_2) to form fully disordered $MgTi_2O_5$ at an extrapolated temperature of 1860 °C.

Keywords: Crystal structure, high-temperature, neutron diffraction, order-disorder, oxides, karrooite, rutile, geikielite

Introduction

Pseudobrookite (Fe_2TiO_5) provides the type structure (space group 63, *Cmcm*) for a chemically wide-ranging group of both mineral and synthetic metal oxides with the general formula AB_2O_5 (Bayer 1971; Bowles 1988). Its crystal structure consists of edge-shared MO_6 octahedra, with two non-equivalent octahedral sites, M1 (4*c*) and M2 (8*f*), occurring in the ratio 1:2 (Pauling 1930); the M1 site is larger and more distorted than the M2 site (Fig. 1a). Pseudobrookite-type minerals have been found in volcanic and in highly oxidized metamorphic rocks, and were identified in lunar basalts (Anderson et al. 1970) formed from Ti-rich, reduced magmas. Armalcolite, the pseudobrookite-structured lunar mineral, was named for the first lunar explorers, and Mg-rich Karroo volcanics in South Eastern Zimbabwe and South Africa have provided members of the solid solution $MgTi_2O_5$–Fe_2TiO_5 (Cox and Hornung 1966).

The pseudobrookite structure-type is populated by chemically diverse end-members which include Ga_2TiO_5, Al_2TiO_5 (tieilite), $CoTi_2O_5$, Fe_2TiO_5, $MgTi_2O_5$, $FeTi_2O_5$, Sc_2TiO_5, and Ti_3O_5, all of which have been found to be thermodynamically stable at high temperatures only. This unusual property has been proposed to arise from entropy stabilization, with positive enthalpies of formation (ΔH) from simpler oxides being offset by larger, positive entropy of formation terms ($T\Delta S$), resulting in negative free energies of formation (Navrotsky 1975).

Pseudobrookite-type phases will thus decompose upon slow cooling to single or mixed oxides, or to a lower symmetry phase, as found for Ti_3O_5 (Onoda 1998). The temperature above which these phases are stable varies according to composition. For $Fe^{2+}Ti_2O_5$, this temperature is 1140 ± 10 °C, below which $FeTiO_3$ and TiO_2 are stable; for $Fe_2^{3+}TiO_5$, the assemblage Fe_2O_3 + TiO_2 is stable below 565 °C. Substitution of Mg for Fe in the $MgTi_2O_5$–$FeTi_2O_5$ solid solution lowers the decomposition temperature (Pownceby and Fisher-White 1999). Thus quenching of some pseudobrookite-type compositions is possible. Although $Fe_{0.5}Mg_{0.5}Ti_2O_5$ decomposes below 1010 ± 20 °C, the presence of Al_2TiO_5, Cr_2TiO_5, and Ti_3O_5 in solid solution in armalcolite, ($Fe_{0.5}Mg_{0.5}Ti_2O_5$) may reduce the decomposition temperature (Kesson and Lindsley 1975).

Solid-solution series include $Fe_2^{3+}TiO_5$–$Fe^{2+}Ti_2O_5$ (Akimoto et al. 1957, Haggerty and Lindsley 1970), $FeTi_2O_5$–Ti_3O_5 (Grey and Ward 1973), and $MgTi_2O_5$–$FeTi_2O_5$ (Moore and Sigurdson 1949; Lindsley et al. 1974), and form under a wide range of oxygen fugacities. Other solid solutions are under investigation, including Sc_2TiO_5–Al_2TiO_5 (Kolitsch and Tillmanns 2003).

A direct corollary of high-*T* stability is that these phases become unstable with increasing pressure. A recent computational study found a hypothetical pseudobrookite-structured Al_2SiO_5 polymorph to be unstable under conditions of the upper mantle (Oganov and Brodholt 2000). Lindsley et al. (1974) showed that $MgTi_2O_5$ breaks down to geikielite + rutile under *P*-*T* conditions matching those of the upper mantle/lower crust, and Borisov et al. (2004) have recently determined the liquidus stability of $MgTi_2O_5$ in an anorthite-diopside eutectic melt.

Because the M1 and M2 octahedral sites within pseudo-

* E-mail: a.lennie@dl.ac.uk

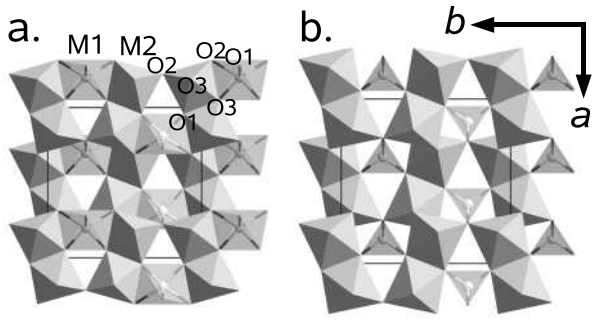

FIGURE 1. (**a**) The crystal structure of $MgTi_2O_5$ (Kar4, 23 °C) projected upon [001]. All atoms lie in the *a*-*b* plane at either *c* or *c*/2. All M-O_6 octahedra share edges in the pseudobrookite-type structure. M1 (2*mm*) and M2 (*m*) sites are labeled. (**b**) The high *T* (Kar4, 1492 °C) structure of $MgTi_2O_5$, with M1 shown as tetrahedra.

brookites are crystallographically distinct, any order/disorder exchange of cations between these sites is a non-convergent process (Thompson 1969). It has been proposed that increasing cation disorder with increasing temperature contributes to the entropy component required for stabilization of pseudobrookite-type phases at high *T* (Waldbaum 1973; Navrotsky 1975). Partitioning of cations between non-equivalent sites in minerals has long been of interest as a possible indicator of geochemical or petrological processes. However, in situ neutron diffraction studies of olivine have shown that rapid site exchange of Mg, Fe, and Mn prevents quenching of cation ordering states from >~700 °C (Henderson et al. 1996; Redfern et al. 1996; Henderson et al. 2001). Cation reordering at lower *T* values may thus reflect post-magmatic thermal histories of olivine-bearing rocks rather than the high *P*-*T* conditions of formation (Redfern et al. 1996). Cation configurations in oxide spinels also change upon heating, becoming increasingly randomly distributed over tetrahedral and octahedral sites (Harrison et al. 1998; Redfern et al. 1999).

In this paper, we report results of an in situ study of the *T* dependence of cation order/disorder between the M1 and M2 sites in pseudobrookite-type structured $MgTi_2O_5$ (karrooite) up to ~1500 °C. The strong contrast between neutron scattering lengths of Mg and Ti, and absence of magnetic ordering, makes this phase ideal for study by neutron diffraction. In addition, there are no redox effects to complicate cation behavior, in contrast to Fe-bearing pseudobrookite phases.

THE STRUCTURE OF $MgTi_2O_5$ (KARROOITE)

Previous work has shown that the room-*T* unit-cell parameters of $MgTi_2O_5$ depend on the annealing *T* and rate of quenching which together control the degree of intersite ordering; the hypothetical fully ordered form has significantly smaller *a*, larger *b*, slightly smaller *c,* and smaller volume, *V* (Hazen and Yang 1997). Bayer (1971) reported thermal expansion coefficients between 20 and 1020 °C of $\alpha_a = 10.8 \times 10^{-6}$ K^{-1}, $\alpha_b = 15.9 \times 10^{-6}$ K^{-1}, and $\alpha_c = 2.3 \times 10^{-6}$ K^{-1}, ($\alpha_V = 29.2 \times 10^{-6}$ K^{-1}), but did not consider the separate effects of thermal expansion and intersite Ti-Mg exchange. Note that the unit-cell axes used by Bayer have been interchanged to be consistent with the *Bbmm* setting of the space group. *Cmcm* (*a*, *b*, *c*) transforms to *Bbmm* (*b*, *c*, *a*).

A single-crystal X-ray structural refinement determined at room *T* for a sample of $MgTi_2O_5$ annealed at 1500 °C (Lind and Housley 1972) showed Mg ordering into M1, with Ti preferentially occupying the smaller and less distorted M2 site. Some cation disorder was established, with 31.6% of Ti occupying M1 sites. X-ray and neutron powder diffraction data obtained from quenched $MgTi_2O_5$ showed cation equilibration to be rapid above ~700 °C, and cation disorder increasing with *T* (Wechsler and Navrotsky 1984; Wechsler and Von Dreele 1989). Brown and Navrotsky (1989) used the room-*T* neutron diffraction structures of Wechsler (1977) for $MgTi_2O_5$ samples quenched from 400 and 1100 °C to develop an empirical model for estimating values of the site occupancy (*x*) of Ti in the M1 site. Their method involves using room-*T* cell parameters (specifically *c*) for samples quenched from 500–1500 °C to deduce values for *x*; they suggested that the Mg-Ti disorder could not be quenched from above 1000 °C. They also estimated *x* from cell parameters determined between 700–1200 °C and extrapolated these estimates for *x* to 1500 °C assuming a linear relationship between *x* and *T*. They used these *x* values, together with high-*T* calorimetric measurements, to calculate thermodynamic data for order-disorder systematics of $MgTi_2O_5$. More recently, thermodynamic models for the pseudobrookite structure have been developed by Ghiorso et al. (1999), calibrated from data of Hazen and Yang (1997) and Yang and Hazen (1999), and by Xirouchakis et al. (2002), using the Brown and Navrotsky (1989) data.

Single-crystal X-ray diffraction studies on $MgTi_2O_5$ quenched to room *T* after annealing at high *T* have been used to predict the unit-cell parameters of fully disordered and fully ordered forms (Yang and Hazen 1998) with the former having the larger volume. Yang and Hazen (1998) show that with increasing cation disorder, the degree of distortion of M1 octahedra reduces significantly, while that of M2 remains essentially unchanged. Because disordered $MgTi_2O_5$ is less dense than ordered $MgTi_2O_5$, a prediction from bulk modulus-volume systematics is that disordered $MgTi_2O_5$ will be more compressible than the ordered phase. Bulk moduli for theoretically fully ordered and disordered $MgTi_2O_5$ have been established by extrapolating room-*T* bulk moduli from four crystals with different *x* (Hazen and Yang 1997). These authors calculated that the differences between ordered and fully disordered bulk moduli are an order of magnitude greater than those predicted from bulk modulus-volume systematics alone. They ascribed this to the effect of cation disorder on M1 and M2 octahedra where the compressibility of disordered $MgTi_2O_5$ is more isotropic and therefore less constrained along **a** and **c** axes.

Most authors have used the Ti occupancy of the M1 site (denoted *x*) to define the cation site occupancy of karroite; because there is only one M1 site the value of *x* is also the mole fraction of Ti in the M1 site (x^{M1}_{Ti}). For stoichiometric $MgTi_2O_5$ the number of Ti cations per formula unit in the M2 site is therefore (2 – *x*). Fully ordered $MgTi_2O_5$ has all Ti in the M2 site with *x* = 0 and the fully disordered form has *x* = 2/3; an anti-ordered phase (M1 fully occupied by Ti) would have *x* = 1. Ghiorso et al. (1999) chose to modify this terminology by defining an order parameter *s* as follows: $s = X^{M1}_{Mg} - 2X^{M2}_{Mg}$, where *X* terms are mole fractions. The fully ordered state has *s* = 1, disordered has *s* = –1/3, and anti-ordered $MgTi_2O_5$ (Ti filling the M1 site) would have *s* = –1. The order parameter defined in this way is related

to x by $s = 1 - 2x$.

Adopting terminology used for intersite order in spinels (Harrison et al. 1998; Redfern et al. 1999) the degree of order for $MgTi_2O_5$ may also be defined as an order parameter Q:

$$Q = X^{M1}_{Mg} - X^{M2}_{Mg},$$

where $Q = 1$ for completely ordered $MgTi_2O_5$, $Q = 0$ for a fully disordered arrangement, and $Q = -0.5$ for the anti-ordered configuration. The relationship between Q and x can be denoted $Q = 1 - 3/2x$.

As would be expected, the degree of disorder increases as T increases and, as has been shown for synthetic olivines (e.g., Henderson et al. 1996, 2001) and spinels (e.g., Harrison et al. 1998; Redfern et al. 1999), the equilibrium order is only easily quenchable from T values below ~700–800 °C. Thus high-T disorder properties for olivine and spinel can only be determined reliably using in situ methods. Brown and Navrotsky (1989) have suggested that $MgTi_2O_5$ disorder cannot be quenched from above 1000 °C but in situ experimental work is required to obtain a reliable closure T for Mg-Ti exchange in $MgTi_2O_5$.

Experimental procedure

Synthesis and sample characterization

Three $MgTi_2O_5$ samples were prepared in 10-g batches. Kar1 and Kar2 were synthesized in air from reagent grade MgO and TiO_2 dried at 200 °C, mixed in stoichiometric proportions, and heated in a Pt crucible in a rising hearth furnace at 1200 °C for 48 h. These batches were cooled, reground, annealed for a further 72 h at 1200 °C, then removed from the furnace and allowed to cool in air. Kar4 was prepared from high purity chemicals and was heated at 1400 °C for 3 days, reground, then heated at 1430 °C for a further 3 days. Before and after the heating experiments, each sample was characterized by X-ray powder diffraction using a Philips PW1060 X-ray diffractometer fitted with a curved crystal graphite monochromator, and using a Cu$K\alpha$ radiation source. Room-T unit-cell parameters were determined using Si as internal standard. In addition, samples were analyzed before and after the heating experiments using a Cameca SX100 electron microprobe with MgO and TiO_2 as primary standards and geikielite ($MgTiO_3$) as a secondary standard. The as-synthesized Kar1 sample has minor amounts of an impurity phase containing Na and Ca with the stoichiometry $Ti_{3.57}Mg_{0.43}Ca_{0.07}Na_{0.70}O_8$ (cf. JCPDS data file sample 44-0007 which has the stoichiometry $Ti_{3.55}Mg_{0.45}Na_{0.90}O_8$). The as-synthesized Kar2 sample contains rutile (TiO_2) and geikielite ($MgTiO_3$) as impurities, while the as-synthesized Kar4 sample contains no detectable geikielite or rutile. However, after the neutron diffraction heating experiments the Kar4 sample shows a small degree of alteration with minor amounts of geikielite occurring at $MgTi_2O_5$ grain boundaries. Some of this geikielite seems to be present at above 1400 °C but most appears to have formed during the stepwise cooling experiments below ~1000 °C.

Because of problems with the water cooling of the furnace during the highest T experiments with Kar2, the sample interacted with ceramics in the furnace forming small amounts of a heterogeneous perovskite (stoichiometry varying from $Ca_{1.92}Mg_{0.04}Ti_{2.02}O_6$ to $Ca_{1.39}Mg_{0.47}Ti_{2.07}O_6$) occurring in interstitial regions between primary $MgTi_2O_5$ grains.

Chemical compositions and unit cell parameters for the $MgTi_2O_5$ samples before and after the heating experiments are given in Table 1.

Neutron diffraction

In situ high-T experiments on $MgTi_2O_5$ powders were carried out on the POLARIS diffractometer of the ISIS spallation source, Rutherford Appleton Laboratory. POLARIS is a medium resolution, time-of-flight high intensity neutron powder diffractometer that allows studies of materials under non-ambient conditions (Hull et al. 1992; Smith et al. 1994). Three separate neutron diffraction runs were made.

The first sample (Kar1) was loaded as a powder into a thin-walled silica tube, placed in a vanadium can, and mounted inside a vanadium furnace assembly, which was evacuated to ~5×10^{-4} mbar; in this furnace temperatures were restricted to 1000 °C and were measured using Type K thermocouples. The second and third samples were pressed to form pellets of the oxide powder. Pellet disks were stacked as a pile, held in a tantalum wire basket, and suspended inside the RISO furnace, which has tantalum elements allowing T values up to 1600 °C to be attained. The RISO furnace assembly was evacuated to ~5×10^{-4} mbar. After the experiments in the RISO furnace it was found that the recorded T of ~1600 °C is likely to have been 100–150° lower than indicated by the W/Re thermocouple. One of us (KSK) had subsequently used the RISO furnace to study the phase transition of $CaTiO_3$ with pressed sample pellets (as in this $MgTi_2O_5$ study) and found that the phase transition occurred at a measured T of ~1330 °C rather than the expected 1240 °C. Further experiments in the same furnace, but with the thermocouple surrounded by a powdered sample, gave the expected transition T. The T values for samples Kar2 and Kar4 have therefore been reduced by a factor of 0.9329 (1240/1330). The reliability of this correction was tested against the volume thermal expansion measured for the impurity rutile in Kar2. From our experiments, we determine a mean volume thermal expansion coefficient for rutile, between 25–1400 °C, of 27.5×10^{-6} K^{-1}, which is in reasonable agreement with the published value of 28.9×10^{-6} K^{-1} (Sugiyama and Takéuchi 1991).

For sample Kar1, diffraction patterns were collected in four 30 m time bins over about two hours at each isothermal T step upon heating (~100 μA of data for each time slot), and over a single 30 m period during cooling. No systematic differences in site occupancy are observed if individual 30 m time bins at each T are refined separately, implying that equilibration of cation order is rapid above ~600 °C relative to the measurement time in this experiment. For Kar2, data were collected for about 80 m (200 μA) at each T and for Kar4, collection times of 90 and 110 m (250 and 300 μA) were used. Neutron flight times are between 2.5 and 19.6 ms, corresponding to d-spacings between 0.4 and 3.2 Å. Data from individual detectors were corrected for electronic noise, normalized against standard spectra from V, and focused using in-house software. No corrections were made for beam attenuations by the furnace or sample, as they were found to be negligible. The data range included around 3500 independent Bragg reflections. The Kar1 sample was heated to $T = 1000$ °C. The second and third samples (Kar2 and Kar4) were heated in steps up to $T = 1600$ °C, which based on the $CaTiO_3$ calibration, was later found to be 130° higher than the real T. For Kar1 and Kar4, measurements were taken upon heating and cooling. Measurements for Kar2 were taken upon heating only.

Analysis of data used full Rietveld refinements in the program GSAS (Larson and Von Dreele 1994) to provide structural information and occupancies of cations in M1 and M2 sites. The background signal was modeled using a 6th-order Chebyshev polynomial. The crystallographic variables were the unit-cell parameters, coordinates of O, Mg, and Ti atoms, occupancies of M1 and M2 sites, and isotropic displacement parameters. The very different neutron scattering properties of Ti and Mg (–3.44 and 5.38 fm) allow site occupancies of these two cations to be established with far greater reliability than can be achieved with X-ray diffraction.

We have used the program IVTON (Balić Žunić and Vicković 1996) and the formula of Swanson and Peterson (1980) to calculate MO_6 polyhedral volumes from $MgTi_2O_5$, geikielite, and rutile unit-cell and atomic positional parameters. Bond angle variance (BAV) and mean bond lengths of these polyhedra were calculated from the listing of bond angles and distances from GSAS. Mean bond lengths are calculated from the six metal-anion bond lengths of each octahedron [Σ(M – O)/6], and quadratic elongation (QE) from [$\Sigma(l_i/l_o)_2$]/6, where l_i is each individual octahedral bond length and l_o is the axis length for a regular octahedron having the same volume as the distorted octahedron (Robinson et al. 1971). BAV is calculated using the twelve O-M-O angles defined by taking adjacent anions and measuring the bond angle (θ) through the central cation of each polyhedron [$\Sigma(\theta - 90)^2$/11] (Robinson et al. 1971).

Results

The compositions of the starting samples are identical and within error of the stoichiometric $MgTi_2O_5$ composition; the compositions of Kar1 and Kar2 after the experiments show no significant changes from the starting values (Table 1). However, in Kar4 the $MgTi_2O_5$ phase after the heating experiments was very slightly more Ti-rich than the starting sample (Table 1) reflecting the fact that a small amount of the more Mg-rich geikielite phase had formed by partial breakdown of the original sample at the highest T values and during the cooling experiments. The room-T cell parameters of the $MgTi_2O_5$ phases before

TABLE 1. Chemical compositions (1σ errors in parentheses) and room-*T* unit-cell parameters (2σ errors) for synthetic $MgTi_2O_5$ samples before and after the neutron diffraction heating experiments

	Kar1 (before)	Kar1 (after)	Kar2 (before)	Kar2 (after)	Kar4 (before)	Kar4 (after)
(wt%)						
MgO	20.6(2)	20.4(1)	20.5(1)	20.3(1)	20.4(1)	20.0(1)
TiO_2	80.5(4)	79.6(2)	79.1(2)	81.1(2)	79.7(2)	81.4(3)
Total*	101.1	100.0	99.6	101.4	100.1	101.4
(cations per 5 O)						
Mg	1.013	1.013	1.020	0.994	1.013	0.987
Ti	1.993	1.993	1.990	2.003	1.994	2.032
Unit-cell parameters						
a (Å)	9.742(4)	9.732(3)	9.740(4)	9.746(3)	9.731(2)	9.742(4)
b (Å)	9.997(3)	9.996(2)	9.989(3)	9.992(2)	9.998(2)	9.991(3)
c (Å)	3.745(2)	3.743(1)	3.745(1)	3.746(2)	3.742(1)	3.747(1)
V (Å^3)	364.71(18)	364.15(15)	364.30(17)	364.83(16)	364.01(10)	364.68(15)

* CaO and FeO were below detection (<0.03%).

and after the heating experiments show only small differences (Table 1).

Crystallographic parameters for $MgTi_2O_5$ from Rietveld refinements are listed in Tables 2, 3a, and 4. All refinements were satisfactorily achieved in space group 63 (*Cmcm*). For consistency with previously published studies on $MgTi_2O_5$, we list our tabulated data in the *Bbmm* setting. Mean bond lengths, octahedral volumes, BAV, and QE are summarized in Table 5[1].

For Kar2, structural parameters for the rutile and geikielite impurities were also derived through multi-phase Rietveld refinement, and are listed in Table 3b. The amount of rutile and geikielite decreased above 1000 °C as reaction in situ formed $MgTi_2O_5$. The mole fractions of rutile and geikielite in Kar2 decreased progressively from ~0.125 each at 1000 °C to ~0.025 each at 1400 °C; the $MgTi_2O_5$ mole fraction increases from 0.875 to 0.975.

DISCUSSION

As the unit-cell parameters of $MgTi_2O_5$ depend on both intersite Ti-Mg disorder and thermal expansion, we will consider separately the variation of cell parameters at room *T* with *x* (Ti in M1) and the dependence of *x* on *T*, before considering the combined effects of disorder and thermal expansion on the cell parameters.

Dependence of $MgTi_2O_5$ room-temperature unit-cell parameters on *x*.

Our room-*T* unit-cell parameters and values for *x*, combined with data from the literature (Wechsler and Navrotsky 1984; Wechsler and Von Dreele 1989; Brown and Navrotsky 1989; Yang and Hazen 1998), are displayed in Figures 2a–2d. Note that while 2σ errors for unit-cell edges are around 0.02–0.04% (relative), those for *x* are significantly larger (~1% relative). Indeed, some published *x* values are deduced from cell parameters rather than being determined directly (Brown and Navrotsky 1989) and could be subject to even greater errors. The scatter of points is within 2σ error.

Yang and Hazen (1998) obtained theoretical cell parameters for fully ordered ($x = 0$) and disordered ($x = 2/3$) states by extrapolating data for 5 samples which were rapidly quenched from *T* values between 600 to 1400 °C. These authors showed that *a* and *b* vs. *x* define linear trends while *c* and *V* show negative curvature (positive departures from Vegard's Law, which states that unit-cell parameters of solid solutions of isomorphous substances are linearly dependent on concentration); disorder leads to increased values for *a*, *c*, and *V* but to a reduced *b* cell edge (Fig. 2b) (e.g., Wechsler and Navrotsky 1984; Yang and Hazen 1998). The relative changes in cell parameters between the fully ordered and disordered forms are *a*: +0.77%, *b*: –0.62%, *c*: +0.44%, and *V*: +0.59%. The data for our samples, and for all the published data, confirm that the *a* vs. *x* trend is linear, and that *c* shows clear negative curvature but that *b* shows a slight tendency toward positive curvature. The overall effect on *V* is to show negative curvature equivalent to positive departures from Vegard's Law.

Because of the significant departures from ideality exhibited by different cell parameters, and the relative sensitivities of their variation with site order, we suggest that if room-*T* cell edges are to be used to predict *x*, the most reliable approach would be to use *a* rather than *c* which was used by Brown and Navrotsky (1989); Yang and Hazen (1998) suggested that *a* and *b* are equally useful. Thus we suggest the linear relationship $x = 8.6909a - 84.334$ ($R^2 = 0.96$) as the most reliable way of extracting values of *x* from room-*T* cell parameters.

Temperature dependence of *x*

The dependences of *x* with *T* for our samples are shown in Figure 3. This diagram shows clearly that the starting samples have different *x* values at room *T*, with Kar2 being least ordered (x ~0.34), Kar1 slightly more ordered (x ~0.3), and Kar4 most ordered (x ~0.16). These differences must reflect different effective degrees of cooling from the final annealing *T*. No attempt was made to produce very high quench rates following synthesis.

With increasing *T*, none of the three samples show significant changes in Ti-Mg ordering until the *T* approaches 650 °C, at which point Kar1 and Kar2 begin to show trends toward lower *x* values, i.e., exchange of Ti into M2 and Mg into M1. However, a slight but systematic trend of increasing order is perceptible

[1] Deposit item AM-07-022, Table 5 (mean bond lengths, octahedral volumes, BAV, and QE are summarized). Deposit items are available two ways: For a paper copy contact the Business Office of the Mineralogical Society of America (see inside front cover of recent issue) for price information. For an electronic copy visit the MSA web site at http://www.minsocam.org, go to the American Mineralogist Contents, find the table of contents for the specific volume/issue wanted, and then click on the deposit link there.

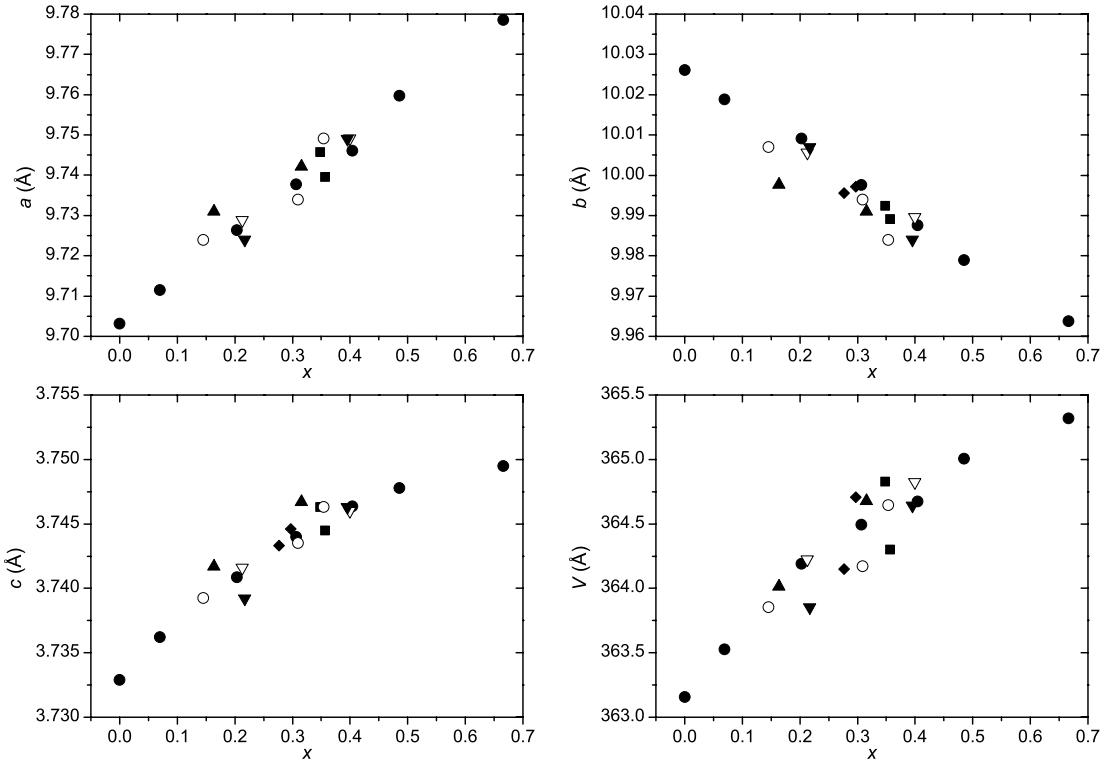

FIGURE 2. Variation of unit-cell parameters (*a, b, c, V*) of $MgTi_2O_5$ with site occupancy (Ti in M1) at room *T*. Data from Kar1, Kar2, and Kar4 are shown by filled diamonds, squares, and triangles, respectively. Data from Yang and Hazen (1998) are shown by filled circles, Wechsler and Navrotsky (1984) by filled inverted triangles, Wechsler and Von Dreele (1989) by open inverted triangles, and Brown and Navrotksy (1989) by open circles.

in Kar1 and Kar2 up to 650 °C. There may be a small degree of site exchange taking place even at these low *T* values. Kar1 achieves its most ordered state (x ~0.24) at around 750 °C, while Kar2 reaches this point (x ~0.31) at ~800 °C. As *T* values are increased further both samples begin to disorder, defining parallel trends with the increasing trend in x for Kar1 being displaced to slightly higher *T* values (~50 °C) than that for Kar2. On cooling, Kar1 shows a similar trend on cooling, without the minimum in x being detected, with the room-*T* cooled sample being slightly more ordered (x ~0.27) than the starting sample. No cooling data are available for Kar2.

These order/disorder trends are characteristic of *T*-dependent site exchange, as has been shown by in situ work on Mg-Mn, Fe-Mn, and Ni-Mg olivines (Henderson et al. 1996, 2001; Redfern et al. 1996) and spinel (Redfern et al. 1999), and have been interpreted as follows. The constant x at low *T* reflects the slow kinetics of site exchange below ~650 °C. Above this *T*, Ti and Mg begin to diffuse between adjacent M1 and M2 sites, moving toward more ordered configurations which are closer to the equilibrium degree of order at these *T* values. Above ~800 °C the exchange rates are now fast enough for the measured x values to represent the equilibrium degree of order for each *T* step and the trend for Kar2 reliably defines these equilibrium states up to 1300 °C. On cooling Kar1, the equilibrium ordering state cannot be maintained below ~700 °C with the measured x value becoming essentially constant below this *T*.

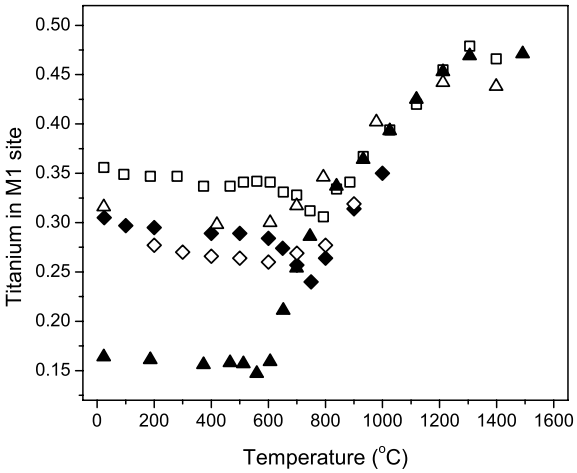

FIGURE 3. *T* dependence of x (Ti in M1) for $MgTi_2O_5$. Data from $Kar1_{heat}$, $Kar1_{cool}$, Kar2, $Kar4_{heat}$, and $Kar4_{cool}$ are shown as filled and open diamonds, open squares, and filled and open triangles, respectively.

The low *T* trend for the most ordered sample Kar4 is slightly different. The x value remains constant at ~0.16 up to ~570 °C at which point it shows a very small decrease—which is unlikely to be significant—and then the sample starts to disorder with x showing a steady increase up to 800 °C where the trend joins that of Kar2. The highest *T* point for Kar2 and the two highest *T* points for Kar4 (>1300 °C) fall at slightly lower values of x

TABLE 2. Refined unit-cell parameters of $MgTi_2O_5$ (Kar1) in *Bbmm* setting, space group 63

$MgTi_2O_5$	Cell parameters				Positional parameters and site occupancies					
Kar1					M1 site (4*c*)	Fraction of	M2 site (8*f*)		Fraction of	O1 site (4*c*)
T (°C)	*a* (Å)	*b* (Å)	*c* (Å)	*V* (Å^3)	M1x	Mg in M1	M2x	M2y	Ti in M2	O1x
25	9.7424(40)	9.9971(26)	3.7446(16)	364.708(182)						
100	9.74731(17)	10.00801(17)	3.74522(7)	365.350(9)	0.1918(5)	0.702(5)	0.13313(26)	0.56081(29)	0.851(2)	0.77321(16)
200	9.75627(18)	10.02152(18)	3.74672(7)	366.327(10)	0.1909(5)	0.705(5)	0.13337(27)	0.56092(30)	0.852(2)	0.77314(16)
400	9.77560(18)	10.04994(18)	3.74966(7)	368.382(10)	0.1892(6)	0.711(5)	0.13369(28)	0.56070(32)	0.855(3)	0.77295(18)
500	9.78490(19)	10.06402(18)	3.75079(7)	369.361(10)	0.1880(6)	0.711(5)	0.13394(29)	0.56067(33)	0.855(3)	0.77293(18)
600	9.79414(19)	10.07788(19)	3.75167(7)	370.305(10)	0.1872(6)	0.716(5)	0.13422(30)	0.56090(34)	0.858(3)	0.77293(19)
650	9.79832(19)	10.08590(19)	3.75201(7)	370.792(10)	0.1870(6)	0.726(6)	0.13421(30)	0.56099(34)	0.863(3)	0.77327(19)
700	9.80182(19)	10.09572(19)	3.75216(7)	371.300(10)	0.1869(6)	0.743(6)	0.13409(29)	0.56102(33)	0.872(3)	0.77405(20)
750	9.80608(19)	10.10545(19)	3.75247(7)	371.850(10)	0.1868(6)	0.760(6)	0.13406(29)	0.56150(33)	0.880(3)	0.77466(20)
800	9.81491(20)	10.11234(20)	3.75402(8)	372.593(11)	0.1856(7)	0.736(6)	0.13431(31)	0.56130(40)	0.868(3)	0.77323(21)
900	9.83298(21)	10.12583(21)	3.75670(8)	374.044(11)	0.1828(9)	0.685(6)	0.13470(40)	0.56000(40)	0.843(3)	0.77072(22)
1000	9.84993(22)	10.14123(22)	3.75870(8)	375.458(12)	0.1801(11)	0.650(7)	0.13540(40)	0.55890(50)	0.825(3)	0.76832(24)
900	9.83300(22)	10.12539(22)	3.75626(8)	373.984(12)	0.1834(9)	0.681(7)	0.13490(40)	0.55980(40)	0.841(3)	0.77035(24)
800	9.81612(21)	10.11187(21)	3.75351(8)	372.571(11)	0.1855(7)	0.723(6)	0.13412(34)	0.56060(40)	0.862(3)	0.77294(22)
700	9.80371(21)	10.09661(20)	3.75150(8)	371.339(11)	0.1869(7)	0.731(6)	0.13396(32)	0.56100(40)	0.866(3)	0.77375(21)
600	9.79268(20)	10.08152(20)	3.74975(8)	370.194(11)	0.1875(6)	0.740(6)	0.13379(31)	0.56150(40)	0.870(3)	0.77414(20)
500	9.78238(20)	10.06691(20)	3.74815(8)	369.112(11)	0.1887(6)	0.736(6)	0.13375(30)	0.56132(34)	0.868(3)	0.77394(20)
400	9.77197(20)	10.05182(19)	3.74664(8)	368.018(11)	0.1893(6)	0.734(5)	0.13355(29)	0.56096(33)	0.867(3)	0.77401(19)
300	9.76162(20)	10.03672(19)	3.74527(8)	366.942(11)	0.1908(5)	0.730(5)	0.13341(28)	0.56138(32)	0.865(3)	0.77409(18)
200	9.75184(20)	10.02262(19)	3.74388(8)	365.923(12)	0.1914(5)	0.723(5)	0.13325(27)	0.56102(31)	0.862(2)	0.77417(17)

Note: The M1 site (4*c*) is *x*,0.25,0; the M2 site (8*f*) is *x*,*y*,0. Occupancies of the O1 (4*c*), O2 (8*f*), and O3 (8*f*) sites are 1. Room-*T* data are from a powder X-ray diffraction measurement.

than the main trend, which suggests a change in behavior such as an unquenchable second order phase transition. Other structural parameters also show discontinuities above 1300 °C, which we discuss in Section 5.5. On cooling, *x* values for Kar4 decrease, within error, along the equilibrium ordering trend, until about 800 °C when the cooled sample stabilizes with $x \sim 0.27$, significantly more disordered than the starting sample. We believe that the as-synthesized Kar4 sample is much closer to a low *T* equilibrium order condition than Kar1 and Kar2 and that this explains the absence of a minimum in its *T* dependence trend. Thus, once the *T* increased beyond the point at which significant site exchange is initiated (~650 °C), Kar4 began to approach the equilibrium order-disorder curve.

The data sets for Kar2 heated above 800 °C and for Kar4 heated above 600 °C fall on the same trend and define a reliable equilibrium order trend from ~700–1300 °C. However, the equilibrium data for Kar1 are displaced from this trend by about 50 °C. Kar1 was studied in a different furnace to Kar2 and Kar4 and there is clearly a problem with correlating the *T* scales of the two furnaces; in any case, data for Kar1 are only available to 1000 °C. We consider therefore that the high-*T* equilibrium order-disorder trend is best described by the data from Kar2 and Kar4 during heating.

Our values for *x* at high *T* show significant differences from those deduced by Brown and Navrotsky (1989) which they based on in situ *c* cell parameters measured from 700–1200 °C and linearly extrapolated to 1500 °C (their Fig. 9), although the values are in reasonable agreement at the lowest *T* values. These substantial discrepancies at the highest *T* values will lead to significant differences in the thermodynamic properties of cation disorder derived for $MgTi_2O_5$ (see Section 5.8). In contrast, our in situ data for *x* are in excellent agreement with values of Yang and Hazen (1998) for samples quenched from 800, 1000, and 1400 °C (their Fig. 3) suggesting that, with extremely fast cooling rates, the Mg-Ti exchange can even be quenched from 1400 °C. This is substantially higher than the maximum quenching *T* of 1000 °C suggested by Brown and Navrotsky (1989). The Yang and Hazen samples quenched from lower *T* values (600 and 700 °C) have *x* values that are significantly smaller than our values. It is likely that the very long equilibration times used by Yang and Hazen (up to 42 days) provide the best estimates of equilibrium degree of order at these *T* values. We have therefore used their data to assign estimates for the effective quench *T* values of our as-synthesized samples as follows: Kar1 800 °C, Kar2 890 °C, Kar4 660 °C. After the in situ heating experiments, the equivalent quench *T* values are 770, 860, and 810 °C, respectively.

Dependence of unit-cell parameters on temperature

The variations of unit-cell parameters with *T* are shown in Figure 4. Based on the results of the previous section, it is clear that unit-cell parameters will be affected by only thermal expansion effects below ~600 °C and by both thermal expansion and intersite cation exchange above this *T*. The trends are further complicated by different ordering paths followed during heating and cooling cycles at low *T* values.

The heating trends are most clearly seen for Kar2 where no cooling experiments were carried out (Fig. 4). The relationships for Kar4 shown in Figure 4 are more complicated because data are available for both heating and cooling experiments; prior to neutron studies, this sample was significantly more ordered than when measured at room *T* following heating in the diffraction furnace (see Fig. 3).

For Kar2, the *a* cell parameter shows two segments with different rates of linear expansion, with the two trends intersecting at ~700 °C; mean thermal expansion coefficients (α) for the two segments are given in Table 6.The slope of the lower *T* segment ($\alpha_a = 10.6 \times 10^{-6}$ K^{-1}) is significantly smaller than that for the higher *T* region ($\alpha_a = 16.6 \times 10^{-6}$ K^{-1}). For *V*, the low-*T* and high-*T* regions have mean expansion coefficients $\alpha_V = 29.9 \times 10^{-6}$ K^{-1} and 36.6×10^{-6} K^{-1}, respectively. For *b* and *c*, the expansion trends are fairly continuous over the whole *T* range. For Kar4, the expansion coefficients for the low-*T* region (25–600

TABLE 2.—*EXTENDED*

O2 site (8*f*)		O3 site (8*f*)		Thermal Parameters (B_{iso})					*x*
O2x	O2y	O3x	O3y	M1(4*c*)	M2(8*f*)	O1(4*c*)	O2(8*f*)	O3(8*f*)	Ti in M1
0.04676(12)	0.11489(11)	0.31243(11)	0.06722(12)	1.015(66)	0.314(36)	0.863(25)	0.831(19)	0.632(17)	0.295(5)
0.04681(13)	0.11476(12)	0.31245(12)	0.06727(12)	1.203(73)	0.383(40)	0.989(27)	0.984(21)	0.750(18)	0.295(5)
0.04698(14)	0.11462(13)	0.31232(13)	0.06743(14)	1.653(89)	0.497(45)	1.273(32)	1.261(25)	1.005(22)	0.289(5)
0.04710(15)	0.11452(13)	0.31215(14)	0.06747(14)	1.871(96)	0.550(48)	1.416(35)	1.416(28)	1.154(24)	0.289(5)
0.04712(16)	0.11448(14)	0.31209(14)	0.06752(15)	2.036(100)	0.597(51)	1.560(37)	1.532(30)	1.266(27)	0.284(5)
0.04715(16)	0.11439(14)	0.31198(15)	0.06726(15)	2.170(110)	0.659(52)	1.623(39)	1.590(30)	1.337(28)	0.274(6)
0.04703(16)	0.11418(14)	0.31209(15)	0.06711(15)	2.216(99)	0.681(51)	1.676(40)	1.661(32)	1.405(28)	0.257(6)
0.04694(16)	0.11405(14)	0.31213(15)	0.06673(16)	2.268(96)	0.749(51)	1.724(40)	1.720(33)	1.477(30)	0.240(6)
0.04724(17)	0.11425(15)	0.31167(16)	0.06736(16)	2.520(111)	0.745(56)	1.813(43)	1.823(36)	1.567(32)	0.264(6)
0.04752(19)	0.11445(16)	0.31114(17)	0.06846(17)	3.025(115)	0.734(69)	2.015(49)	1.972(40)	1.692(36)	0.314(6)
0.04795(21)	0.11467(18)	0.31046(18)	0.06935(19)	3.546(197)	0.692(81)	2.189(54)	2.162(45)	1.862(40)	0.350(7)
0.04771(20)	0.11451(17)	0.31097(18)	0.06846(18)	2.982(159)	0.684(72)	2.016(52)	1.992(43)	1.702(38)	0.319(7)
0.04694(19)	0.11415(16)	0.31177(17)	0.06759(18)	2.445(121)	0.712(62)	1.827(47)	1.805(38)	1.567(34)	0.277(6)
0.04698(18)	0.11418(16)	0.31220(16)	0.06727(17)	2.208(111)	0.658(57)	1.695(43)	1.679(36)	1.425(32)	0.269(6)
0.04694(17)	0.11424(15)	0.31231(15)	0.06707(16)	2.010(100)	0.648(53)	1.522(40)	1.507(32)	1.272(28)	0.260(6)
0.04703(16)	0.11436(14)	0.31238(15)	0.06711(15)	1.739(92)	0.562(49)	1.383(36)	1.386(30)	1.123(26)	0.264(6)
0.04690(15)	0.11444(14)	0.31227(14)	0.06712(14)	1.607(172)	0.489(92)	1.265(69)	1.273(60)	1.000(47)	0.266(5)
0.04685(15)	0.11458(13)	0.31242(13)	0.06706(14)	1.290(78)	0.426(43)	1.117(30)	1.105(25)	0.857(22)	0.270(5)
0.04676(14)	0.11455(13)	0.31247(13)	0.06690(13)	1.057(70)	0.345(40)	0.959(28)	0.987(23)	0.738(20)	0.277(5)

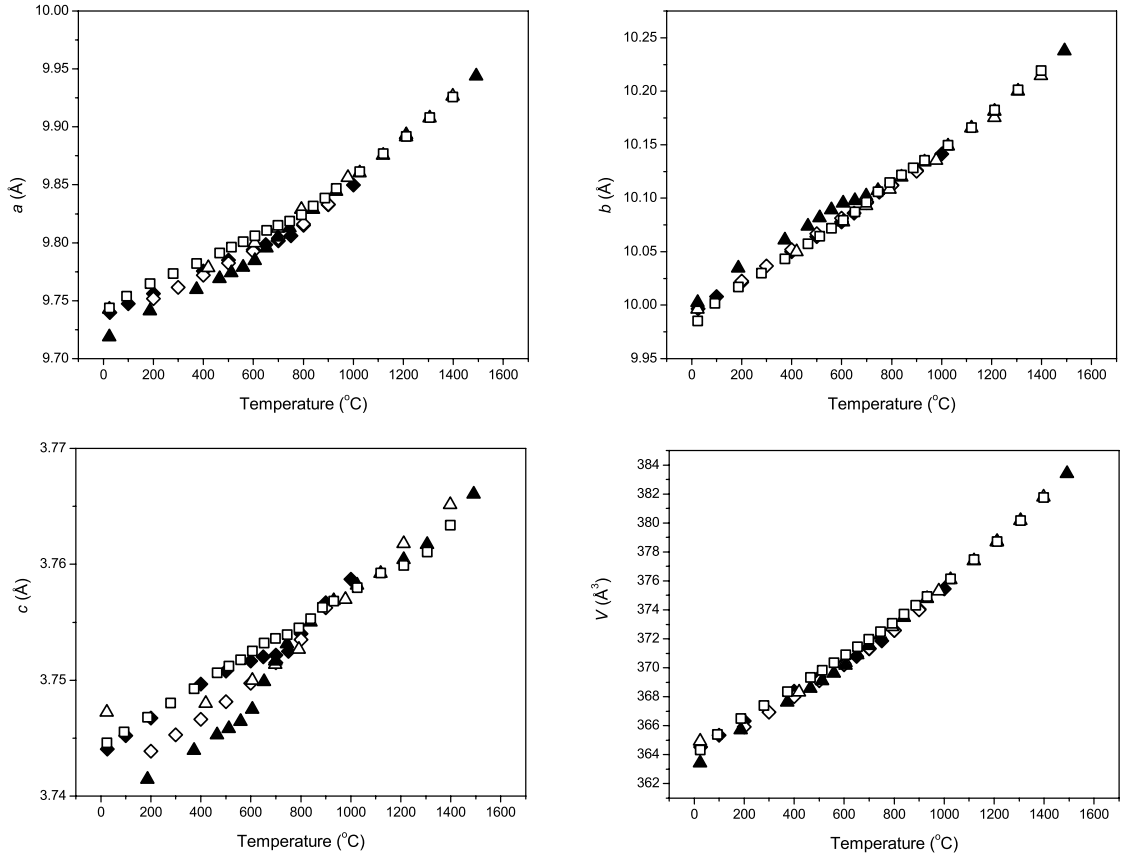

FIGURE 4. *T* dependence of unit-cell parameters (*a, b, c, V*), showing effects of variation in site disorder on unit-cell parameters of $MgTi_2O_5$. Data from $Kar1_{heat}$, $Kar1_{cool}$, Kar2, $Kar4_{heat}$, and $Kar4_{cool}$ are shown as filled and open diamonds, open squares, and filled and open triangles, respectively.

°C) are very similar to those for Kar2 for all the cell parameters. However, the cell parameters (especially *c*) between 600 and 800 °C show a gradual change before the essentially linear high-*T* trend is reached. For Kar4, the cell parameters obtained during the cooling cycle below about 700 °C are greater than those for the heating data, reflecting increased disorder compared with the initial Kar4 sample. It is clear that differences between the heating and cooling cycles of Kar4 reflect the contrast between the cooling path taken during initial synthesis and that taken during the stepwise cooling in the diffraction furnace (Figs. 2

TABLE 3A. Refined unit-cell parameters of $MgTi_2O_5$ (Kar2) in *Bbmm* setting, space group 63

$MgTi_2O_5$ Kar2	Cell parameters				Positional parameters and site occupancies					
					M1 site (4*c*)		M2 site (8*f*)			O1 site (4*c*)
T (°C) corr.	*a* (Å)	*b* (Å)	*c* (Å)	*V* (Å^3)	M1x	Frac. of Mg in M1	M2x	M2y	Frac. of Ti in M2	O1x
23	9.74366(31)	9.98531(31)	3.74460(11)	364.325(19)	0.1951(8)	0.644(5)	0.1329(4)	0.5598(5)	0.822(3)	0.77031(20)
93	9.75392(32)	10.00174(31)	3.74553(11)	365.400(20)	0.1933(9)	0.651(5)	0.1327(4)	0.5599(5)	0.825(3)	0.77000(21)
187	9.76471(33)	10.01702(32)	3.74682(11)	366.489(20)	0.1925(9)	0.653(5)	0.1332(4)	0.5593(5)	0.826(3)	0.77032(22)
280	9.77334(33)	10.03012(32)	3.74802(11)	367.410(20)	0.1922(10)	0.653(6)	0.1336(4)	0.5595(5)	0.827(3)	0.76994(22)
373	9.78228(34)	10.04332(33)	3.74927(11)	368.353(21)	0.1908(10)	0.663(6)	0.1337(4)	0.5595(5)	0.831(3)	0.77013(23)
466	9.79115(34)	10.05724(34)	3.75064(12)	369.333(21)	0.1911(10)	0.663(6)	0.1337(5)	0.5593(5)	0.831(3)	0.77000(24)
513	9.79623(32)	10.06429(31)	3.75121(11)	369.840(20)	0.1906(10)	0.659(5)	0.1343(4)	0.5590(5)	0.830(3)	0.76973(23)
559	9.80114(34)	10.07178(33)	3.75177(12)	370.356(21)	0.1892(10)	0.658(6)	0.1341(5)	0.5594(5)	0.829(3)	0.76981(24)
606	9.80599(35)	10.07940(34)	3.75252(12)	370.893(22)	0.1892(11)	0.659(6)	0.1341(5)	0.5591(5)	0.829(3)	0.76983(25)
653	9.81088(35)	10.08736(35)	3.75321(12)	371.440(22)	0.1899(11)	0.669(6)	0.1340(5)	0.5589(5)	0.835(3)	0.76986(26)
699	9.81498(35)	10.09619(35)	3.75360(12)	371.959(22)	0.1891(11)	0.672(6)	0.1340(5)	0.5589(5)	0.836(3)	0.77054(26)
746	9.81860(34)	10.10618(35)	3.75395(12)	372.499(22)	0.1885(10)	0.688(6)	0.1336(4)	0.5598(5)	0.844(3)	0.77130(26)
793	9.82397(35)	10.11481(36)	3.75450(12)	373.076(22)	0.1881(11)	0.694(6)	0.1341(5)	0.5596(5)	0.847(3)	0.77129(27)
839	9.83183(35)	10.12187(36)	3.75532(13)	373.716(23)	0.1886(12)	0 666(6)	0.1340(5)	0.5586(5)	0.833(3)	0.77049(27)
886	9.83876(36)	10.12856(37)	3.75630(13)	374.325(23)	0.1871(13)	0.659(7)	0.1352(5)	0.5580(6)	0.829(3)	0.76893(28)
932	9.84676(37)	10.13524(38)	3.75683(13)	374.929(24)	0.1857(15)	0.633(7)	0.1349(6)	0.5576(6)	0.817(3)	0.76848(29)
1026	9.86152(37)	10.14961(39)	3.75799(14)	376.139(25)	0.1846(19)	0.606(7)	0.1359(6)	0.5570(7)	0.803(4)	0.76727(30)
1119	9.87714(37)	10.16588(40)	3.75924(14)	377.465(25)	0.1873(25)	0.580(8)	0.1372(6)	0.5555(7)	0.790(4)	0.76510(32)
1212	9.89190(36)	10.18253(39)	3.75989(14)	378.713(24)	0.1835(32)	0.545(8)	0.1372(7)	0.5551(7)	0.773(4)	0.76392(33)
1305	9.90817(36)	10.20140(40)	3.76106(15)	380.157(25)	0.182(4)	0.521(8)	0.1369(7)	0.5542(7)	0.760(4)	0.76228(33)
1399	9.92590(41)	10.21945(45)	3.76338(17)	381.747(29)	0.160(4)	0.534(9)	0.1365(8)	0.5552(8)	0.767(5)	0.76090(40)

Notes: The M1 site (4*c*) is *x*,0.25,0; the M2 site (8*f*) is *x*,*y*,0. Occupancies of O1 (4*c*), O2 (8*f*), and O3 (8*f*) sites are 1.

and 3). Because Kar1 was only studied up to 1000 °C, the high-*T* expansion coefficient can only be estimated from 800–900 °C; nevertheless the data for our three samples are quite similar. However, we prefer to use the more complete data sets for Kar2 and Kar4 to provide the mean expansion coefficients for $MgTi_2O_5$ shown in Table 6.

Our low-*T* mean thermal expansion coefficients are slightly larger than those of Bayer (1971) between 20–520 °C but are in the same order (Table 6). Our in situ data can also be compared with those obtained from the high-*T* unit cell data reported by Brown and Navrotsky (1989). Their room-*T* data for the sample quenched from 973 K, and their in situ data at 973 K, have been used to define the expansion coefficient from 25–700 °C, while their in situ data at 1073 and 1473 K define the expansion coefficient from 800 to 1200 °C (Table 6). Our thermal expansion data show good agreement with the values deduced from the work of Brown and Navrotsky (1989) for both low- and high-*T* expansion coefficients (Table 6). The low-*T* expansion coefficients are very similar for all the $MgTi_2O_5$ samples, irrespective of the distribution of Mg and Ti over the M1 and M2 sites (*x* varies from 0.16–0.35).

At high *T* (>800 °C) all cell parameters for Kar2 and Kar4 show essentially the same trends (Fig. 4), except for the anomalously high values of the three highest *T* *c* cell parameters, which suggest the presence of a phase transition at >1300 °C.

As *x* shows little or no variation up to ~650 °C the low *T* coefficients (denoted α^T) define rates of cell expansion due only to thermal expansion (Table 6). We have also estimated a value for α^T by combining room-T data for a fixed *x* value of 0.404 (Yang and Hazen 1998) with our cell parameters for Kar4, which has $x = 0.404$ at ~1060 °C. The α^T values determined in this way are very similar to the other estimates (Table 6). The higher *T* regions (>700 °C) define the effects of both thermal expansion and increasing disorder but the effect of disorder alone is simply obtained by subtracting the low *T* expansion coefficients from those for the higher *T* region (Table 6). Thus, the mean expansion coefficients for Kar2 and Kar4 for the effects of disorder alone (denoted α^D) over the *T* range 800 to 1300 °C are: α^D_a 6.0 × 10^{-6} K^{-1}, α^D_b 1.1 × 10^{-6} K^{-1}, α^D_c –0.3 × 10^{-6} K^{-1}, and α^D_V 6.9 × 10^{-6} K^{-1}. Over this *T* range *x* increased from 0.30 to 0.48.

Octahedral changes with *T* and disorder.

Bond lengths. Figure 5 shows the variation of mean M1-O and M2-O bond lengths with increasing *T* for all our $MgTi_2O_5$ samples; note that, to improve clarity, data obtained during cooling experiments are shown only for Kar4. At low *T* values, Kar4 is the most ordered sample, with relatively less Ti in M1 and more in M2 than Kar1 and 2. This compositional difference is reflected in mean M1-O and M2-O bond lengths in Kar4, which are greater and smaller respectively than those in Kar1 and 2. Bearing in mind that at low *T* values there is no significant change in the degree of order, it is clear that mean bond-length increases up to about 600–700 °C are due to thermal effects alone.

The mean M1-O thermal expansion coefficients calculated over the *T* range 25–700 °C for our three samples are very similar, as are those for the mean M2-O bonds (Table 6) and demonstrate that the larger M1 site (MgO_6) has a higher thermal expansion rate than that for M2 (TiO_6) (see Section 5.6). At higher *T* values, where Mg^{2+} and Ti^{4+} are now exchanging between the two sites, the mean M1-O bond length shows a contraction while M2-O continues to increase, but at a higher rate than that at low *T*. Note that the high-*T* contraction coefficient for M1-O in Kar1 is much less reliable than those for Kar2 and 4 because Kar1 was only studied up to 1000 °C. Above 1300 °C, the M1-O mean bond lengths show marked discontinuities for both Kar2 and Kar4 but the M2-O values lie on the same trend. Figure 6 shows the changes for individual M-O distances in both M1 and M2 polyhedra, normalized to the value at room *T* in each case; no room-*T* structural data are available for Kar1 in the furnace and it is assumed that the bond lengths at 25 °C are the same as those for

TABLE 3A.—*EXTENDED*

O2 site (8*f*)		O3 site (8*f*)		Thermal Parameters (B_{iso})					*x*
O2x	O2y	O3x	O3y	M1(4*c*)	M2(8*f*)	O1(4*c*)	O2(8*f*)	O3(8*f*)	Ti in M1
0.04658(17)	0.11502(14)	0.31229(16)	0.06831(16)	0.312(75)	1.341(146)	0.878(43)	0.775(36)	0.689(33)	0.356(5)
0.04654(18)	0.11500(15)	0.31199(17)	0.06819(17)	0.435(81)	1.779(161)	1.074(42)	1.016(30)	0.903(28)	0.349(5)
0.04654(19)	0.11474(16)	0.31205(18)	0.06832(18)	0.555(89)	1.941(171)	1.209(46)	1.180(32)	1.067(31)	0.347(5)
0.04666(20)	0.11474(16)	0.31200(18)	0.06827(18)	0.632(92)	2.295(181)	1.365(47)	1.318(33)	1.162(32)	0.347(6)
0.04663(21)	0.11460(17)	0.31190(19)	0.06849(19)	0.668(94)	2.592(187)	1.478(51)	1.445(36)	1.269(33)	0.337(6)
0.04665(22)	0.11431(18)	0.31207(20)	0.06839(19)	0.746(100)	2.781(197)	1.560(53)	1.617(39)	1.405(36)	0.337(6)
0.04649(21)	0.11453(16)	0.31190(19)	0.06840(18)	0.793(096)	2.925(190)	1.668(51)	1.711(36)	1.472(34)	0.341(5)
0.04663(22)	0.11426(18)	0.31194(20)	0.06830(19)	0.816(103)	2.801(196)	1.790(55)	1.787(39)	1.523(36)	0.342(6)
0.04645(23)	0.11434(18)	0.31200(21)	0.06826(20)	0.824(107)	3.095(211)	1.849(58)	1.865(41)	1.635(39)	0.341(6)
0.04677(24)	0.11433(19)	0.31174(21)	0.06820(21)	0.856(108)	3.345(215)	1.877(59)	1.915(43)	1.645(39)	0.331(6)
0.04613(24)	0.11399(19)	0.31207(22)	0.06809(21)	0.864(107)	3.118(203)	1.904(60)	2.004(43)	1.700(39)	0.328(6)
0.04595(24)	0.11400(19)	0.31260(22)	0.06773(21)	0.910(104)	3.407(197)	1.987(61)	2.041(43)	1.777(40)	0.312(6)
0.04630(25)	0.11377(20)	0.31202(23)	0.06732(22)	1.057(111)	3.413(202)	2.081(65)	2.182(46)	1.833(42)	0.306(6)
0.04617(25)	0.11398(20)	0.31203(23)	0.06795(22)	0.975(117)	3.601(227)	2.187(66)	2.264(47)	1.903(43)	0.334(6)
0.04674(27)	0.11408(21)	0.31131(23)	0.06827(23)	1.131(132)	4.106(260)	2.246(69)	2.369(49)	1.930(44)	0.341(7)
0.04675(27)	0.11428(21)	0.31132(24)	0.06881(23)	0.936(138)	4.348(299)	2.332(73)	2.461(51)	2.066(47)	0.367(7)
0.04683(29)	0.11434(22)	0.31083(25)	0.06900(24)	0.929(157)	5.112(378)	2.568(77)	2.654(54)	2.195(48)	0.394(7)
0.04747(30)	0.11469(23)	0.30991(26)	0.07006(25)	0.832(178)	6.418(518)	2.670(81)	2.794(57)	2.292(50)	0.420(8)
0.04686(32)	0.11465(23)	0.30942(26)	0.07004(25)	0.601(191)	6.713(645)	2.957(85)	3.118(61)	2.440(51)	0.455(8)
0.04746(33)	0.11479(24)	0.30866(26)	0.07106(26)	0.157(179)	6.739(752)	3.066(84)	3.306(64)	2.571(53)	0.479(8)
0.0478(4)	0.11507(27)	0.30849(30)	0.07096(30)	0.133(204)	8.258(1024)	2.910(94)	2.861(67)	2.356(60)	0.466(9)

TABLE 3B. Refined unit-cell parameters of $MgTiO_3$ (geikielite) in space group 148 and TiO_2 (rutile) in space group 136

Rutile *T* (°C)	*a*	*c*	*V* (Å³)	Octahedral Volume (Å³) Ti-O6	Geikielite *T* (°C)	*a*	*c*	*V* (Å³)	Octahedral Volume (Å³) Ti-O6	Mg-O6
23	4.59225(31)	2.95756(32)	62.371(9)	9.813	23	5.05425(41)	13.89550(201)	307.401(57)	9.759	12.300
93	4.59613(31)	2.96157(32)	62.561(9)	9.844	93	5.05943(41)	13.91393(203)	308.440(57)	9.794	12.415
186	4.60068(32)	2.96478(33)	62.753(9)	9.849	186	5.06437(42)	13.93426(209)	309.494(59)	9.779	12.487
280	4.60344(31)	2.96782(32)	62.893(9)	9.878	280	5.06866(41)	13.94909(207)	310.349(58)	9.783	12.519
373	4.60685(32)	2.97044(32)	63.042(9)	9.900	373	5.07315(41)	13.96171(208)	311.180(58)	9.927	12.431
466	4.61051(33)	2.97312(34)	63.199(10)	9.908	466	5.07743(43)	13.97990(216)	312.112(61)	9.897	12.451
513	4.61194(31)	2.97425(32)	63.262(9)	9.912	513	5.08006(39)	13.98751(201)	312.605(56)	9.983	12.486
559	4.61414(32)	2.97576(33)	63.355(9)	9.953	559	5.08329(42)	13.99482(215)	313.166(60)	9.930	12.577
606	4.61539(34)	2.97771(35)	63.431(10)	9.942	606	5.08482(44)	14.00640(225)	313.614(63)	9.974	12.495
653	4.61700(34)	2.97898(35)	63.502(10)	9.960	653	5.08748(44)	14.01329(228)	314.097(64)	9.930	12.608
699	4.61894(34)	2.98104(35)	63.599(10)	9.969	699	5.08967(43)	14.02777(222)	314.692(62)	9.968	12.606
746	4.62062(34)	2.98241(35)	63.675(10)	9.970	746	5.09255(43)	14.03480(223)	315.206(63)	10.000	12.609
792	4.62270(35)	2.98386(36)	63.763(10)	9.976	792	5.09549(44)	14.04110(232)	315.712(65)	9.992	12.582
839	4.62472(36)	2.98515(37)	63.846(11)	9.976	839	5.09832(44)	14.05138(232)	316.294(65)	9.981	12.603
886	4.62623(37)	2.98640(38)	63.915(11)	9.997	886	5.10149(45)	14.05776(239)	316.831(67)	9.947	12.644
932	4.62797(38)	2.98819(38)	64.001(11)	10.019	932	5.10317(45)	14.07050(240)	317.327(67)	10.126	12.576
1026	4.63089(40)	2.99074(40)	64.137(12)	10.017	1026	5.10888(48)	14.09022(258)	318.484(72)	9.997	12.667
1119	4.63547(44)	2.99384(44)	64.330(13)	10.045	1119	5.11431(53)	14.10827(289)	319.570(80)	9.888	12.822
1212	4.63821(58)	2.99725(57)	64.480(17)	10.049	1212	5.12081(72)	14.12930(409)	320.860(113)	9.888	12.882
1305	4.64026(161)	3.00032(154)	64.603(46)	10.068	1305	5.13544(280)	14.10452(1700)	322.130(461)	9.936	12.932
1398	4.61303(543)	3.00994(503)	64.052(151)		1398	5.11837(657)	14.29863(4191)	324.396(1118)		

Note: Volumes calculated for rutile Ti-O6 octahedra, and geikielite Ti-O6 and Mg-O6 octahedra are also listed.

100 °C. For the M1 octahedron in all of our samples at *T* values up to ~600 °C, M1-O3 shows the largest thermal expansion increase, M1-O1 a smaller increase, and M1-O2 a clear decrease (Figs. 6a, 6c, and 6e); between 600 and 800 °C the M1-O2 distances in Kar1 and 2 define a maximum, see Figure 6a in particular. In contrast, for the M2 octahedron up to ~600 °C in Kar1 and Kar2 and to ~550 °C in Kar4, M2-O1 and M2-O2' distances show a small thermal expansion, M2-O2 a very small expansion, and M2-O3 and M2-O3' show little or no change (Figs. 6b, 6d, and 6g). For Kar1 and Kar2 between 600 and 800 °C, M2-O1 and M2-O2' define a minimum, and M2-O3 a maximum, in their expansion trends (Figs. 6b and 6d). The *T* range showing points of inflection—maxima or minima—in some of the individual M-O distances is that where cation exchange is initiated, with the amount of Ti in M1 first decreasing and then increasing (Fig. 3), and with the complementary trend of Mg decreasing in M2 prior to subsequent increase. Thus the changes seen in individual M1-O and M2-O bond-lengths reflect these cation exchange systematics. Above 800 °C, the dimensional changes are now affected by both thermal expansion and increasing order (increasing Ti in M1 coupled to increasing Mg in M2). For this higher *T* region the main changes are that now the M1-O2 length decreases faster while M2-O1 and M2-O2' lengths show significant increases, with that for M2-O1 in Kar4 being particularly large. In addition, M2-O2 and M2-O3 bond lengths show clear decreases. These trends are clearly related to the onset of disordering at ~800 °C in Kar2 and ~600 °C in Kar4 (Figs. 6c–6f). Again, above 1300 °C, both Kar4 and Kar2 show discontinuities for some of the individual M1-O bond-lengths, but not for M2-O. M1-O1 and M1-O3 both show significant jumps to higher values and M1-O2

TABLE 4. Refined unit-cell parameters of $MgTi_2O_5$ (Kar4) in Bbmm setting, space group 63

$MgTi_2O_5$	Cell parameters				Positional parameters and site occupancies					
Kar4					M1 site (4*c*)		M2 site (8*f*)			O1 site (4*c*)
T (°C)	*a* (Å)	*b* (Å)	*c* (Å)	*V* (Å^3)	M1x	Frac. of Mg in M1	M2x	M2y	Frac. of Ti in M2	O1x
23	9.71870(16)	10.00247(15)	3.73850(5)	363.423(9)	0.19560(22)	0.836(3)	0.13215(16)	0.56452(19)	0.918(1)	0.77786(11)
186	9.74142(17)	10.03457(16)	3.74144(6)	365.729(10)	0.19459(25)	0.839(3)	0.13223(18)	0.56457(21)	0.919(1)	0.77803(13)
373	9.75978(17)	10.06098(17)	3.74393(6)	367.628(11)	0.19361(28)	0.844(3)	0.13219(19)	0.56438(22)	0.922(1)	0.77811(14)
466	9.76908(18)	10.07391(17)	3.74530(6)	368.586(11)	0.19301(28)	0 842(3)	0.13251(20)	0.56388(23)	0.921(1)	0.77799(14)
513	9.77408(18)	10.08166(17)	3.74584(6)	369.111(11)	0.19318(29)	0.843(3)	0.13258(20)	0.56434(23)	0.921(2)	0.77824(14)
559	9.77881(19)	10.08928(18)	3.74643(6)	369.627(11)	0.19274(31)	0.853(3)	0.13214(21)	0.56426(25)	0.927(2)	0.77846(15)
606	9.78484(19)	10.09554(18)	3.74748(6)	370.188(11)	0.19248(32)	0.841(3)	0.13233(21)	0.56391(25)	0.920(2)	0.77781(15)
653	9.79543(19)	10.09778(19)	3.74989(7)	370.909(12)	0.19070(40)	0.789(3)	0.13232(24)	0.56311(28)	0.894(2)	0.77538(16)
699	9.80486(21)	10.10195(20)	3.75167(7)	371.596(13)	0.19020(50)	0.746(3)	0.13203(28)	0.56236(32)	0.873(2)	0.77370(17)
746	9.81305(21)	10.10736(21)	3.75313(7)	372.251(13)	0.18880(50)	0.714(4)	0.13207(30)	0.56173(35)	0.857(2)	0.77237(17)
839	9.82881(22)	10.11972(21)	3.75501(8)	373.491(14)	0.18780(70)	0.663(4)	0.13190(34)	0.56050(40)	0.832(2)	0.77004(18)
932	9.84426(22)	10.13377(22)	3.75685(8)	374.781(14)	0.18640(80)	0.636(4)	0.13230(40)	0.55900(40)	0.818(2)	0.76827(19)
1026	9.86015(23)	10.14863(23)	3.75822(8)	376.074(15)	0.18480(100)	0.607(4)	0.13180(40)	0.55880(50)	0.803(2)	0.76653(20)
1119	9.87542(22)	10.16546(23)	3.75922(8)	377.381(14)	0.18230(130)	0.575(4)	0.13190(50)	0.55770(50)	0.788(2)	0.76544(21)
1212	9.89149(23)	10.18141(25)	3.76040(9)	378.707(16)	0.18090(160)	0.547(4)	0.13300(50)	0.55570(50)	0.773(2)	0.76395(22)
1305	9.90790(24)	10.20019(26)	3.76172(10)	380.169(17)	0.17610(210)	0.531(5)	0.13190(50)	0.55560(60)	0.766(3)	0.76217(25)
1492	9.94405(33)	10.23771(36)	3.76606(14)	383.401(23)	0.14570(220)	0.529(8)	0.13370(80)	0.55270(80)	0.764(4)	0.75930(40)
1398	9.92655(37)	10.21475(40)	3.76514(15)	381.775(26)	0.15190(240)	0.562(9)	0.13210(80)	0.55320(90)	0.781(5)	0.76250(40)
1212	9.89323(32)	10.17544(34)	3.76179(13)	378.692(22)	0.17810(290)	0.558(7)	0.13190(70)	0.55650(70)	0.779(4)	0.76481(32)
979	9.85621(30)	10.13525(30)	3.75696(11)	375.302(19)	0.18620(170)	0.598(6)	0.13230(50)	0.56000(60)	0.799(3)	0.76781(26)
792	9.82879(28)	10.10848(28)	3.75267(10)	372.843(18)	0.18860(100)	0.654(5)	0.13240(40)	0.56170(50)	0.827(2)	0.77082(22)
699	9.81259(29)	10.09296(28)	3.75135(10)	371.526(18)	0.18860(90)	0.683(5)	0.13200(40)	0.56290(50)	0.842(2)	0.77258(22)
606	9.79992(28)	10.07775(28)	3.74997(10)	370.351(18)	0.18980(80)	0.700(4)	0.13240(40)	0.56230(40)	0.850(2)	0.77319(22)
420	9.77836(32)	10.04989(31)	3.74801(11)	368.322(20)	0.19320(80)	0.702(5)	0.13180(40)	0.56330(50)	0.851(3)	0.77386(24)
23	9.74266(11)	9.99620(11)	3.74724(4)	364.942(7)	0.19370(28)	0.684(2)	0.13255(16)	0.56364(19)	0.842(1)	0.77420(9)

Notes: The M1 site (4*c*) is *x*,0.25,0; the M2 site (8*f*) is *x*,*y*,0. Occupancies of the O1 (4*c*), O2 (8*f*), and O3 (8*f*) sites are 1.

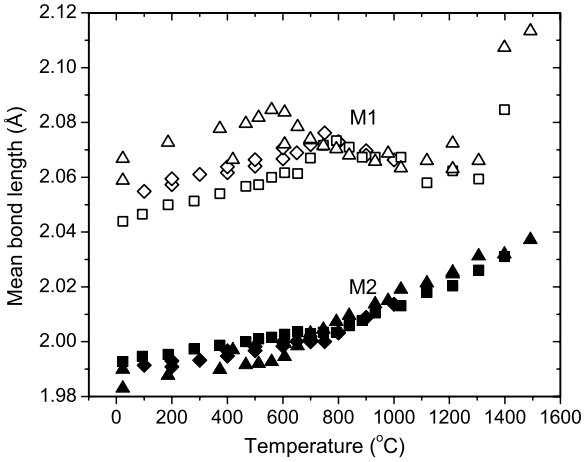

FIGURE 5. Mean bond lengths of M1 and M2 octahedra in $MgTi_2O_5$: Kar1 (diamonds), Kar2 (squares), and Kar4 (triangles); M1 (open symbols), M2 (filled symbols). The divergence of mean bond length for the M1 site at high *T* is discussed in the text.

to lower values (Figs. 6c–6f).

Octahedral parameters. Figures 7 and 8 show how QE and BAV (Robinson et al. 1971) vary as a function of *T*. The M1 site is considerably more distorted than the M2 site as shown by both dimensional (Fig. 7) and angular distortion parameters (Fig. 8). At *T* values up to 600–700 °C, the effect of thermal expansion is to show a slight increase in QE for M1 with very little change in M2, and to show clear increases in the BAV for M1 (Fig. 8a). No significant change is seen for M2. Note that QE and BAV for M1 in Kar4 are larger than those for Kar1 and 2 (Fig. 8b), reflecting the higher content of larger Mg in the former, more ordered sample, but the *T* trends are parallel. Of all the structural parameters considered, the BAV data show the clearest rate of change at the *T* values where the samples have attained the equilibrium degree of disorder, i.e., ~700 °C in Kar4 and ~800 °C in Kar1 and Kar2 (Fig. 8b). Above these *T* values, both QE and BAV for M1 start to decrease while those for M2 show a small increase. Above 1300 °C, while both QE and BAV for the M1 octahedron show distinct discontinuities with higher degrees of distortion, M2 shows absolutely no change in trend for these parameters.

Displacive phase transition >1300 °C

Above 1300 °C, Kar2 and Kar4 both show structural parameter changes that define distinct discontinuities. Above these discontinuities *x* decreases, *c* parameters are slightly larger, M1-O1 and M1-O3 bond-lengths are larger, M1-O2 bond lengths are smaller, and QE and BAV values for M1 are significantly larger.

Inspecting M1 from the refinements at 1492 and 1398 °C, we note that the M1-O3 bond lengthens significantly, from 2.26 to 2.45 Å (Fig. 6) and bond angles O1-M1-O1 and O2-M1-O2 converge toward 109° while O1-M1-O2 remains at about 107°. In effect, the oxygen coordination of the M1 site changes significantly from a very distorted octahedral to a pseudo-tetrahedral coordination (Fig. 1b). At the same time, the angle between metals in adjacent octahedral M2-M1-M2 linkages increases from ~163° to ~173°.

While the M1 octahedron displays these well-defined structural effects, much less change occurs for M2. Data for Kar4 are available from both heating and cooling experiments. On cooling Kar4 below 1300 °C, the various parameters revert to the values measured for the heating runs between 1300 and 800 °C. Taking the data for Kar2 and Kar4 together it seems likely that these discontinuities arise from an unquenchable, second-order displacive phase transition between 1300 and 1400 °C.

TABLE 4.—*EXTENDED*

O2 site (8*f*)		O3 site (8*f*)		Thermal Parameters (B_{iso})					
O2x	O2y	O3x	O3y	M1(4*c*)	M2(8*f*)	O1(4*c*)	O2(8*f*)	O3(8*f*)	x (Ti in M1)
0.04598(9)	0.11428(8)	0.31344(8)	0.06479(9)	0.244(32)	0.032(24)	0.482(19)	0.344(13)	0.287(13)	0.164(3)
0.04573(10)	0.11423(9)	0.31355(10)	0.06498(10)	0.541(40)	0.215(29)	0.772(23)	0.687(17)	0.580(17)	0.161(3)
0.04570(11)	0.11393(9)	0.31340(11)	0.06498(11)	0.826(47)	0.401(34)	0.991(26)	0.924(19)	0.803(18)	0.156(3)
0.04564(12)	0.11404(10)	0.31341(11)	0.06507(11)	0.899(48)	0.490(36)	1.112(28)	1.069(21)	0.917(20)	0.158(3)
0.04572(12)	0.11387(10)	0.31349(12)	0.06485(11)	0.937(50)	0.445(36)	1.124(28)	1.135(21)	1.004(21)	0.157(3)
0.04555(13)	0.11381(11)	0.31362(13)	0.06471(12)	0.912(53)	0.477(39)	1.057(31)	1.026(22)	0.902(22)	0.147(3)
0.04560(13)	0.11388(11)	0.31364(13)	0.06513(12)	1.157(56)	0.550(40)	1.308(32)	1.205(23)	1.085(22)	0.159(3)
0.04589(13)	0.11410(11)	0.31307(13)	0.06595(12)	1.424(68)	0.643(47)	1.408(34)	1.331(24)	1.154(23)	0.211(3)
0.04593(15)	0.11455(12)	0.31242(14)	0.06669(13)	1.614(84)	0.692(55)	1.553(37)	1.416(26)	1.225(25)	0.254(3)
0.04626(15)	0.11441(12)	0.31225(14)	0.06736(14)	1.797(98)	0.732(62)	1.638(39)	1.484(27)	1.293(26)	0.286(4)
0.04637(16)	0.11470(13)	0.31189(15)	0.06797(14)	1.957(122)	0.666(71)	1.816(42)	1.694(29)	1.434(28)	0.337(4)
0.04665(17)	0.11487(14)	0.31146(16)	0.06863(15)	2.490(155)	0.707(84)	1.968(46)	1.853(32)	1.605(30)	0.364(4)
0.04673(18)	0.11530(14)	0.31085(16)	0.06923(16)	3.011(199)	0.959(103)	2.187(49)	2.058(34)	1.713(32)	0.393(4)
0.04657(19)	0.11500(15)	0.31068(17)	0.06971(16)	3.206(244)	0.776(113)	2.315(51)	2.294(36)	1.869(33)	0.425(4)
0.04711(20)	0.11524(16)	0.31001(18)	0.07029(17)	3.589(315)	0.403(121)	2.523(55)	2.393(39)	2.039(36)	0.453(4)
0.04716(22)	0.11542(17)	0.30988(19)	0.07080(18)	4.474(427)	0.461(144)	2.800(62)	2.587(43)	2.130(38)	0.469(5)
0.04740(29)	0.11513(23)	0.30963(29)	0.07108(27)	5.029(782)	0.469(226)	2.863(91)	2.268(58)	2.047(55)	0.471(8)
0.04784(31)	0.11483(24)	0.31040(30)	0.07022(28)	5.911(776)	0.695(231)	2.525(95)	1.744(56)	1.660(56)	0.438(9)
0.04657(28)	0.11522(21)	0.31133(25)	0.06958(23)	6.654(586)	0.600(178)	2.602(77)	2.126(50)	1.893(47)	0.442(7)
0.04628(24)	0.11507(18)	0.31164(21)	0.06811(20)	4.765(349)	0.837(134)	2.326(65)	2.049(42)	1.751(39)	0.402(6)
0.04610(20)	0.11497(16)	0.31219(19)	0.06713(18)	3.267(194)	0.651(93)	1.923(54)	1.657(36)	1.491(35)	0.346(5)
0.04590(20)	0.11479(16)	0.31251(18)	0.06632(18)	2.781(163)	0.667(85)	1.731(52)	1.508(35)	1.364(34)	0.317(5)
0.04562(19)	0.11465(15)	0.31255(18)	0.06633(17)	2.239(138)	0.533(75)	1.614(49)	1.343(32)	1.233(32)	0.300(4)
0.04576(20)	0.11499(16)	0.31280(19)	0.06618(18)	1.772(144)	0.324(75)	1.398(51)	1.018(33)	0.923(32)	0.298(5)
0.04636(7)	0.11478(7)	0.31273(7)	0.06611(7)	0.692(38)	0.172(21)	0.653(13)	0.609(9)	0.527(9)	0.316(2)

TABLE 6. Mean thermal expansion coefficients for unit-cell parameters and M-O bond lengths for M1 and M2 octahedra in $MgTi_2O_5$ derived from these experiments, and compiled from literature sources

Sample or data source	*T* range (°C)	α_a (×10^6)	α_b (×10^6)	α_c (×10^6)	α_v (×10^6)	M1	M2
Kar1	100–600	9.66	14.02	3.52	27.3	11.34	8.64
	800–900	17.84	14.28	6.23	38.45	–1.59	25.43
Kar2	25–606	10.6	15.52	3.61	29.9	13.99	8.18
	793–1305	16.61	16.51	3.3	36.64	–12.68	21.11
Kar4	25–559	11.28	15.76	3.91	31.01	15	8.67
	839–1305	17.22	17.03	3.68	38.12	–5.03	22.24
Mean Kar2 and Kar4	25–600	10.94	15.64	3.76	30.46	14.5	8.43
	800–1300	16.92	16.77	3.49	37.38	–8.86	21.68
Bayer (1971)	20–520	8.1	13.2	2.3	23.61		
Brown and Navrotsky (1989)	25–700	11.12	13.47	4.6	29.19		
	800–1200	19.87	16.81	4.48	41.16		
Yang and Hazen (1998) and this work for *x* fixed at 0.404	25–1060	11.79	16.2	3.12	31.3	24.15	18.84

Molar volume controls of the reaction karrooite = rutile + geikielite

Our as-synthesized sample Kar2 contains impurities of rutile and geikielite in addition to karrooite. Cell parameters for all three phases have been determined allowing the relative volumes of these phases to be compared directly at each *T* step. Using these volume data and the number of formula units (Z) in the unit cell (rutile 2, geikielite 6, and karrooite 4), molar volumes as a function of *T* can be calculated. The molar volumes for both rutile and geikielite show almost linear expansion rates from 25 to 1300 °C: $V_{rutile} = 0.000517T + 18.784$ ($r^2 = 0.999$) and $V_{geikielite} = 0.001119T + 30.814$ ($r^2 = 0.997$). Over this *T* range, rutile and geikielite show no change in structure (geikielite is always fully ordered) and thus the expansion is due to thermal effects alone. We have shown (Fig. 4) that the cell volume for Kar2 shows linear expansion up to 700 °C with no change in degree of order, giving an equation $V_{karrooite} = 0.001646T + 54.834$ ($r^2 = 0.999$). This linear relationship can be extrapolated up to 1400 °C to compare with the data for rutile and geikielite.

The reaction of interest is:

$$MgTi_2O_5 = TiO_2 + MgTiO_3,$$

where

$$\Delta V_{reaction} = V_{karrooite} - V_{rutile} - V_{geikielite}$$

and shows that karrooite is about 10% larger than rutile +

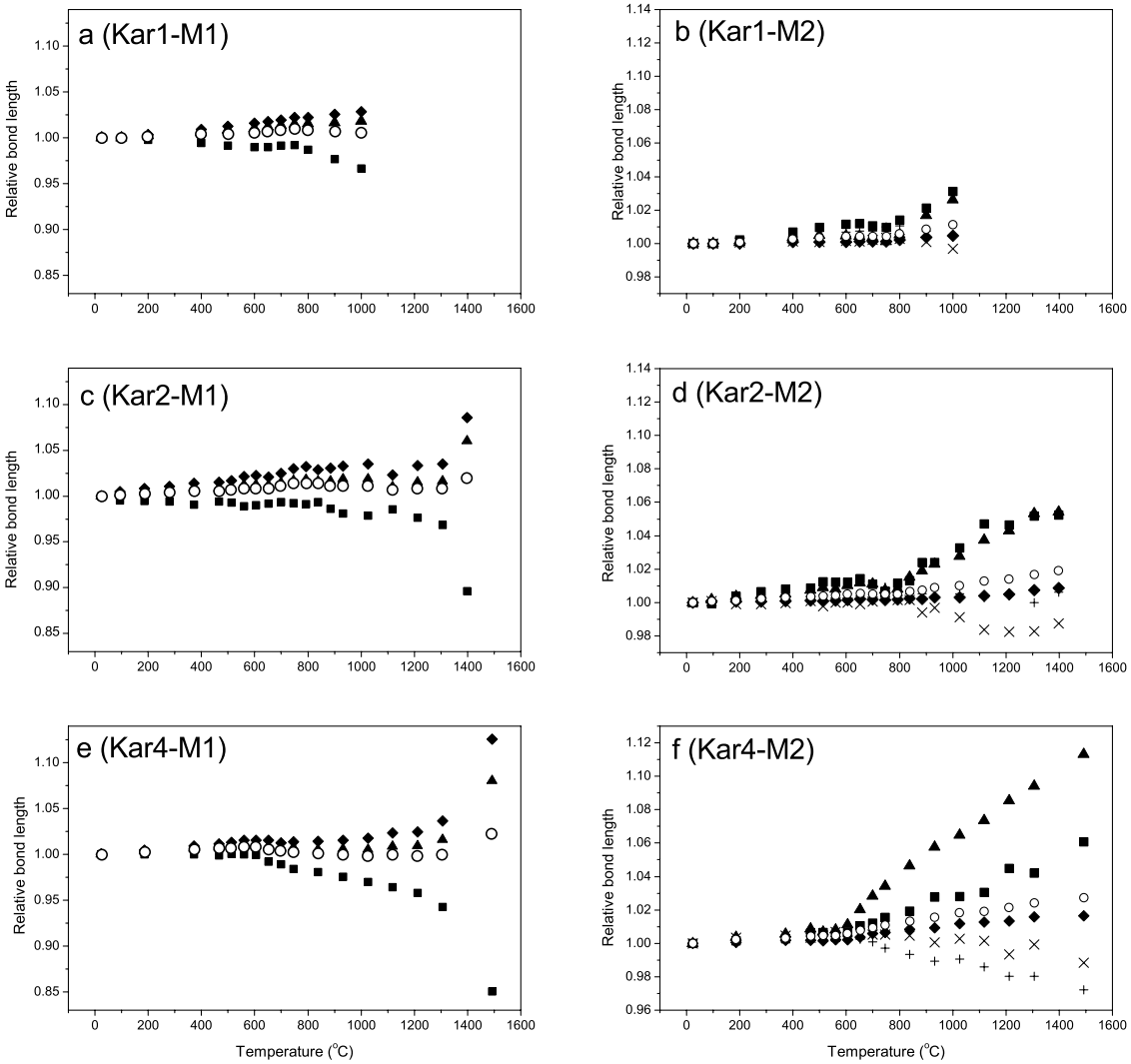

FIGURE 6. Individual M-O distances for M1 and M2 polyhedra normalized to the value at room *T*. In M1, M1-O1 distances are shown by filled triangles, M1-O2 by filled squares, and M1-O3 by filled diamonds. In M2, M2-O1 distances are shown by filled triangles, M2-O2' by fillefil squares, M2-O2 by plus signs, M2-O3 by crosses and M2-O3' by filled diamonds. Mean bond lengths are shown by open circles. Data for heating cycles only are shown.

geikielite (Fig. 9a). The X symbols in Figure 9b show the dependence of $\Delta V_{reaction}$ from 25 to 1300 °C if it is assumed that $MgTi_2O_5$ shows no effects of disorder. Note that $\Delta V_{reaction}$ shows only a very small increase as *T* increases. Thus, changes in vibrational entropy as *T* increases seem to play only a very small part in this reaction. Also shown in Figure 9b are the $\Delta V_{reaction}$ values (solid inverted triangles) calculated using the measured Kar2 volume data from 700–1300 °C instead of values extrapolated from low *T*. These values show the increase in $\Delta V_{reaction}$, due entirely to the effects of Ti-Mg exchange where, as *T* increases, the $MgTi_2O_5$ becomes increasingly disordered. Thus, an additional increase in volume due to disorder provides additional configurational entropy stabilization for $MgTi_2O_5$ at high *T* (Brown and Navrotsky 1989).

At 1300 °C, Kar2 has an *x* value of ~0.48; extrapolating the high-*T* trend for Figure 2 to $x = 0.66$ would give a predicted *T* ~1860 °C for fully disordered $MgTi_2O_5$. Extrapolating the measured $\Delta V_{reaction}$ trend in Figure 9b to 1860 °C then gives an estimate of $\Delta V_{reaction} = 5.92$ cm^3/mol for the maximum stabilization for a fully disordered, but metastable, $MgTi_2O_5$. The extrapolation to lower *T* shows clearly that cation disordering commences at ~650 °C.

Systematics of M-O bond thermal expansion

The primary control on thermal expansion of a cation-anion bond is the interatomic potential between the two ions. In $MgTi_2O_5$, Mg is mainly ordered in M1 and Ti in M2 octahedral sites, both of which are distorted. Hazen et al. (2000) have compared thermal expansion behavior of several MgO_6 octahedra and shown that, despite the wide variety of oxides and silicates in which these octahedra are found, their mean Mg-O bond lengths show very similar rates of thermal expansion. These mean Mg-O bond distances exhibit a coefficient of expansion of ~14(±2) $\times 10^{-6}$ K^{-1}, even though mean bond lengths cover a range from 2.06–2.14 Å (Hazen et al. 2000).

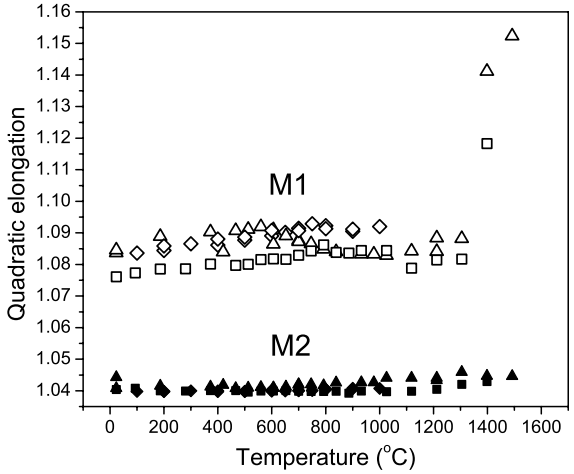

FIGURE 7. *T* evolution of octahedral distortions for M1 (top: open symbols) and M2 (bottom: filled symbols) as shown by quadratic elongation (QE). Data are shown by diamonds (Kar1), squares (Kar2), and triangles (Kar4).

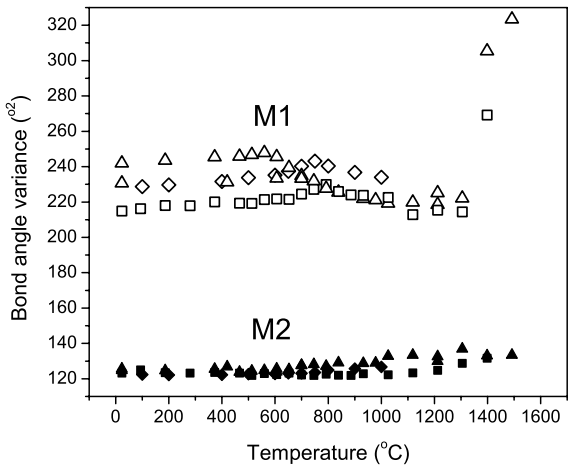

FIGURE 8. *T* dependence of bond angle variance (BAV) for M1 (open symbols) and M2 (filled symbols) as shown by diamonds (Kar1), squares (Kar2), and triangles (Kar4).

A general relation for the coefficient of linear thermal expansion of mean bond lengths (Hazen and Finger 1982) is: $\alpha = 4.0(4)[n/S^2 z_c z_a] \times 10^{-6}$ K^{-1} where S^2 is an empirical ionicity factor, n is the coordination number, and z_c and z_a are the formal cation and anion valencies respectively. For oxides, $S^2 = 0.5$, with α for Mg-O bonds predicted to be ~12×10^{-6} K^{-1}, while α for Ti-O bonds is in the order of ~6×10^{-6} K^{-1}, half that for Mg-O.

In our study, the mean Kar4 M1-O bond length (0.836 Mg: 0.164 Ti) is 2.07 Å at room *T*. Our mean bond length coefficient of thermal expansion up to 600 °C, for a fixed degree of disorder, is 15×10^{-6} K^{-1}, which agrees well with the survey of measured thermal expansions (Hazen et al. 2000). For the M2 site (0.918 Ti:0.082 Mg), the mean bond length expansion up to 600 °C is 8.7×10^{-6} K^{-1}. Above ~650 °C, as Ti^{4+} exchanges into M1, the average bond strength will increase and the coefficient of expansion

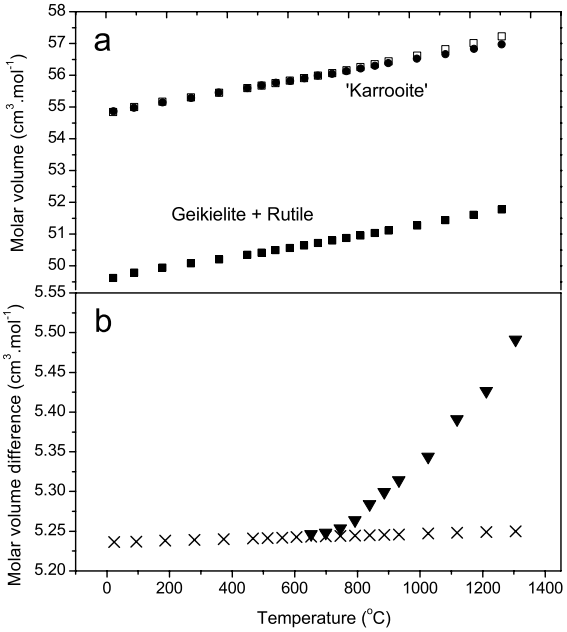

FIGURE 9. Difference in molar volume [K – (G + R)] between $MgTi_2O_5$(K) and component oxides, $MgTiO_3$(G) and TiO_2(R) against *T*. (**a**) The molar volumes of (G + R) and K. The (G + R) molar volume (filled squares) is subtracted from both molar volumes of K calculated from the fit (<700 °C) to the thermal expansion (filled circles) and from molars volume of K measured above 700 °C (open squares). (**b**) These differences [K(fit) – (G + R)] and [K(measured) – (G + R)] are shown by crosses and inverted triangles respectively. The discontinuity in molar volume difference above 700 °C is therefore due to cation disorder.

will decrease. Similarly as Mg^{2+} substitutes into M2, the bond strength will weaken, increasing the coefficient of expansion. Figure 10a shows these trends very clearly.

We note that the M1 and M2 octahedral volumes are identical at ~1150 °C for Mg occupancies of 0.564 in M1 and 0.217 in M2, equivalent to mean cation radii of M1 = 0.81Å and M2 = 0.77Å (based on ionic radii at room *T*). Above 1150 °C, the mean ionic radii in the two sites converge as the site occupancies converge due to increasing disorder, but the sizes of the octahedra diverge with M2 expanding and M1 contracting (Fig. 10a).

In Figure 10b we also show volumes vs. *T* for end-member Ti-O and Mg-O octahedra calculated from the geikielite and rutile present in Kar2. By comparing these data with those for $MgTi_2O_5$ M1 and M2, it is clear that for all *T* values the volume of the Mg-rich M1 site is much smaller than that for a pure Mg-O octahedron, and only slightly larger in volume than that of a pure Ti-O octahedron (Fig. 10b). The clear mismatch between octahedral volumes of $MgTi_2O_5$ M1 and those of geikielite Mg-O octahedra shows that cation behavior in M1 differs from a usual octahedral site.

As the degree of disorder increases, more Ti enters this M1 site and the M1 octahedral volume contracts further, while that for M2 increases (larger Mg entering the smaller M2 site). The M1 site mean bond length reaches a minimum between about 1200–1300 °C before increasing significantly above these *T* values. We note that the U_{iso} for the M1 site is anomalously

large compared to that for M2 (see Table 4) with the trends for U_{iso} vs. T showing a major divergence once the site disordering becomes facile (i.e., larger amounts of small Ti entering M1). This is not a result of the M1 site becoming contrast matched (note that the effective site scattering length for M1 at 1300 °C is 1.154 fm compared to that for M2 of –1.326) and we suggest that a fundamental change is taking place in the geometry of the M1 site, which at higher T is reflected by its change to a tetrahedral-like symmetry.

We have explored several alternative models to explain the anomalously high T factors for the M1 site, including refinement of anisotropic displacement factors for M1 and disordered cation site models. No significant anisotropy was observed for the displacement parameters. Whilst a stable refinement was achieved for a half-atom model with (in *Bbmm*) *x*½*z* (*z* ~0) the magnitude of the *x* displacement was comparable to its associated e.s.d. Alternative models with the site split into *xy*0, *y* ~1/4 and *xyz*, *y* ~1/4, *z* ~0 were unstable. Instead, M1 appears to be behaving more like a tetrahedral site above ~1300 °C, with the four short M1-O bonds (2× ~2.2 Å and 2× ~1.7 Å) forming a tetrahedron, and the two long M1-O bonds (~2.45 Å) indicative of weak bonding to M1 cations (Fig. 11) giving the anomalous increase in mean bond length. This site shows similarities to the behavior of tetrahedral Mg in disordered spinel (Redfern et al. 1999), which has mean Mg-O bond lengths of ~1.92 Å at ~1400 °C. Here, the tetrahedral site decreases in size above ~700 °C as the occupancy of the smaller Al^{3+} cation increases. Although providing much insight into the behavior of $MgTi_2O_5$ at high T, our powder diffraction study does not identify the spatial distribution of Ti and Mg cations in M1. To resolve this issue, a high-T single-crystal study would be required.

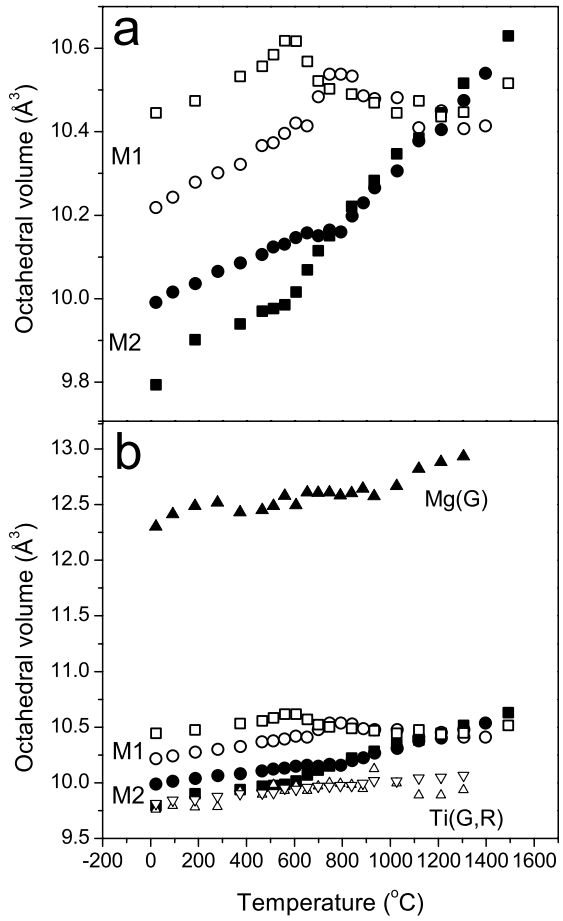

FIGURE 10. (**a**) Octahedral volumes for M1 (Kar2 = open circles; Kar4 = open squares) and M2 (Kar2 = filled circles; Kar4 = filled squares) in $MgTi_2O_5$. (**b**) The octahedral volumes for M1 and M2 are shown with Mg-O_6 and Ti-O_6 volumes from geikielite (filled and open triangles, respectively), and Ti-O_6 volumes from rutile (inverted triangles).

Thermodynamics of intersite exchange

In their study of $MgTi_2O_5$, Wechsler and Navrotsky (1984) used the simple equilibrium model of Navrotsky and Kleppa (1967) in which it is assumed that the enthalpy of cation interchange is independent of the extent of disorder. The cation exchange reaction can be described by:

$$Mg_{M1} + Ti_{M2} = Mg_{M2} + Ti_{M1}$$

where Ti_{M1} refers to the atomic proportion of Ti in site M1, which defines the degree of disorder term x. Because of the stoichiometry of $MgTi_2O_5$ this would lead to an occupancy of x for Mg in M2. Thus the equilibrium constant (K_D) for the reaction is given by: $K_D = x_2/[(1 - x)(2 - x)]$ and the interchange enthalpy (ΔH_{int}) may be calculated from: $K_D = \exp(-\Delta H_{int}/RT)$ where R is the universal gas constant [8.3143 J/(K·mol)].

We have shown that above ~700–800 °C our measured values of x reflect the equilibrium degree of disorder as a function of T. A plot of ln K_D against 1/T (K) defines an Arrhenian relationship with slope $-\Delta H_{int}/R$ and intercept $\Delta S/R$, where ΔS is the non-configurational entropy of disordering. Figure 12 shows the equilibrium data for Kar2 (800–1300 °C) combined with those for Kar4 (750–1300 °C); only data for the heating cycles are included. The fit provides a value for ΔH_{int} = 33.6 kJ/mol and ΔS = 10.7 kJ/(mol·K). Larger values were obtained for Kar1 [39.3

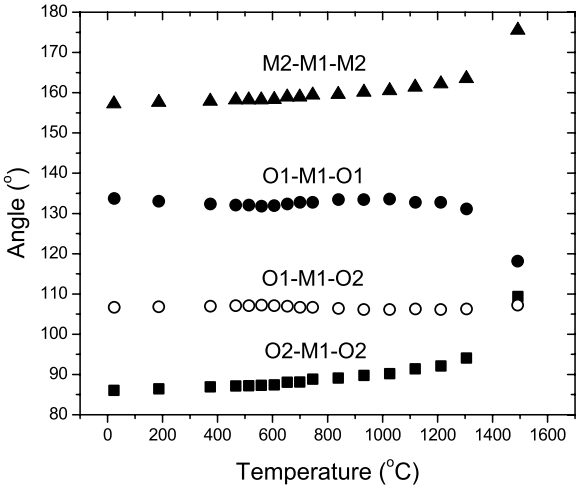

FIGURE 11. Bond angles from Kar4. The M2-M1-M2 angles (triangles) are between cations in M1 and M2 sites. The O1-M1-O1 (filled circles) and O2-M1-O2 (squares) and O1-M1-O2 (open circles) describe the M1-O_4 pseudo-tetrahedron at high T.

kJ/mol and 13.0 kJ/(mol·K)], but these are only based on a very restricted T range (800–1000 °C) and the values we obtain for Kar2 and Kar4 are preferred.

Our estimates for the enthalpy and entropy of Ti-Mg exchange can be compared with those quoted by Brown and Navrotsky (1989) of 47.3 kJ/mol and 2.65 kJ/(mol·K), respectively, although we note that Xirouchakis et al. (2002) concluded the latter value incorrect due to a typographical error, the correct value being closer to 20.6 kJ/(mol·K). To check this suggestion we have fitted Brown and Navrotsky's ΔG_D values for the O'Neill-Navrotsky model (data from their Table 8) and obtain $\Delta H_D = 49.5$ kJ/mol and $\Delta S_D = 24.1$ kJ/(mol·K); the latter value confirms the misprint in their paper. These values are significantly higher than those from our in situ data but were obtained by assuming that the heat capacity does not vary with varying disorder. We have also used Brown and Navrotsky's ΔG_D values for their $\Delta C_{P,D}$ model (their Table 8), in which heat capacity varies with degree of disorder, to obtain values of $\Delta H_D = 40.4$ kJ/mol and $\Delta S_D = 17.5$ kJ/(mol·K), which are in better agreement with our data, but still significantly higher. Our estimates are also lower than those of Xirouchakis et al. (2002) [ΔH_D 42–46 kJ/mol and ΔS_D 15–21 kJ/(mol·K)] but this is to be expected as the Xirouchakis et al. (2002) thermodynamic model is based on the x values proposed by Brown and Navrotsky (1989).

The fact that our in situ data give lower values than Brown and Navrotsky (1989) and Xirouchakis et al. (2002) for both enthalpy and entropy of disordering is directly related to the method used by the former authors to infer values for x from the c cell parameter measured both in quenched samples at room T and in high-T unit-cell data between 700 and 1200 °C (and linearly extrapolated to 1500 °C). We have shown earlier that the highest T x values deduced by Brown and Navrotsky (1989) are substantially higher than our directly determined values (see above) and this leads to substantially higher estimates for the enthalpy of disorder. We have also shown that the steric effects of cation order/disorder on polyhedral geometry and cell parameters are significantly different at high T values to those at room-T (see Figs. 4, 7, and 8 and Table 5[1]) and herein lies the problem in the approach used by Brown and Navrotsky (1989).

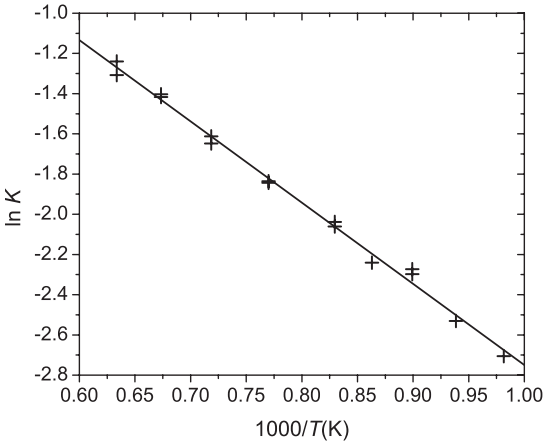

FIGURE 12. Variation of ln K with 1000/T, where K defines the equilibrium cation exchange between M1 and M2 sites above ~973 K. Data are from Kar2 and Kar4 heating measurements only.

Our in situ determinations of x at high T are in excellent agreement with those determined for rapidly quenched samples by Yang and Hazen (1998). The thermodynamic model of Ghiorso et al. (1999), which is based on the structural data of Yang and Hazen, is therefore in much better agreement with our data than that of Xirouchakis et al. (2002).

Experiments at high T on $MgTi_2O_5$ (Lindsley et al. 1974) showed that the stability of $MgTi_2O_5$ decreased with increasing pressure, resulting in breakdown to geikielite and rutile. Instability with high pressure is likely to characterize all pseudobrookite phases, and has been calculated to affect the stability of pseudobrookite-structured Al_2SiO_5 (Oganov and Brodholt 2000). A full thermodynamic understanding of these intriguing phases awaits further measurements of cation ordering and associated structural changes at elevated T and P.

ACKNOWLEDGMENTS

This research was supported by EPSRC/ISIS direct access grants RB9075 and RB10612. We thank Ron Smith for help in setting up POLARIS and David Plant for electron microprobe analyses of the samples.

REFERENCES CITED

Akimoto, S., Nagata, T., and Katsura, T. (1957) The $TiFe_2O_5$–Ti_2FeO_5 solid solution series. Nature, 179, 37–38.

Anderson, A.T., Bunch, T.E., Cameron, E.M., Haggerty, S.E., Boyd F.R., Finger, L.W., James, O.B., Keil, K., Prinz, M., Ramdohr, P., and El Goresy, A. (1970) Armalcolite: a new mineral from the Apollo 11 samples. Proceedings of the Apollo 11 Lunar Science Conference, Geochimica et Cosmochimica Acta, Supplement, 1, 1, 55–63.

Balić Žunić, T. and Vicković, I. (1996) IVTON—program for the calculation of geometrical aspects of crystal structures and some crystal chemical application. Journal of Applied Crystallography, 29, 305–306.

Bayer, G. (1971) Thermal expansion characteristics and stability of pseudobrookite-type compounds, Me_3O_5. Journal of the less-common metals, 24, 129–138.

Borisov, A., Brenker, F., and Palme, H. (2004) Liquidus karrooite stability and composition at reducing conditions. Contributions to Mineralogy and Petrology, 148, 69–78.

Bowles, J.F.W. (1988) Definition and range of composition of naturally occurring minerals with the pseudobrookite structure. American Mineralogist, 73, 1377–1383.

Brown, N.E. and Navrotsky, A. (1989) Structural, thermodynamic, and kinetic aspects of disordering in the pseudobrookite-type compound karrooite, $MgTi_2O_5$. American Mineralogist, 74, 902–912.

Cox, L.G. and Hornung, G. (1966) The petrology of the Karroo Basalts of Basutoland. American Mineralogist, 51, 1414–1432.

Ghiorso, M.S., Yang, H., and Hazen, R.M. (1999) Thermodynamics of cation ordering in karrooite ($MgTi_2O_5$). American Mineralogist, 84, 1370–1374.

Grey, I.E. and Ward, J. (1973) An X-ray and Mössbauer study of the $FeTi_2O_5$-Ti_3O_5 system. Journal of Solid State Chemistry, 7, 300–307.

Haggerty, S.E. and Lindsley, D.H. (1970) Stability of the pseudobrookite (Fe_2TiO_5)–ferropseudobrookite ($FeTi_2O_5$) series. Carnegie Institution of Washington Yearbook, 68, 247–249.

Harrison, R.J., Redfern, S.A.T., and O'Neill, H.St.C. (1998) The temperature dependence of the cation distribution in synthetic hercynite ($FeAl_2O_4$) from in-situ neutron structure refinements. American Mineralogist, 83, 1092–1099.

Hazen, R.M. and Finger, L.W. (1982) Comparative crystal chemistry: temperature, pressure, composition and the variation of crystal structure. John Wiley and Sons, New York.

Hazen, R.M. and Yang, H. (1997) Increased compressibility of pseudobrookite-type $MgTi_2O_5$ caused by cation disorder. Science, 277, 1965–1967.

Hazen, R.M., Downs, R.T., and Prewitt, C.T. (2000) Principles of comparative crystal chemistry. In R.M. Hazen and R.T. Downs, Eds., High-temperature and high-pressure crystal chemistry, 41, p. 11–33. Reviews in Mineralogy and Geochemistry, Mineralogical Society of America, Chantilly, Virginia.

Henderson, C.M.B., Knight, K.S., Redfern, S.A.T., and Wood, B.J. (1996) High-temperature study of octahedral cation exchange in olivine by neutron powder diffraction. Science, 271, 1713–1715.

Henderson, C.M.B., Redfern, S.A.T., Smith, R.I., Knight, K.S., and Charnock, J.M. (2001) Composition and temperature dependence of cation ordering in Ni-Mg olivine solid solutions: a time-of-flight neutron powder diffraction and EXAFS study. American Mineralogist, 86, 1170–1187.

Hull, S., Smith, R.I., David, W.I.F., Hannon, A.C., Mayers, J., and Cywinski, R. (1992) The POLARIS Powder Diffractometer at ISIS. Physica B, 180–181,

1000–1002.
Kesson, S.E. and Lindsley, D.H. (1975) The effects of Al^{3+}, Cr^{3+} and Ti^{3+} on the stability of armalcolite. Proceedings of the 6th Lunar Science Conference, Geochimica et Cosmochimica Acta, Supplement 6, 911–920.
Kolitsch, U. and Tillmanns, E. (2003) Sc_2TiO_5, an entropy-stabilized pseudobrookite-type compound. Acta Crystallographica, E59, i36–i39.
Larson, A.C. and Von Dreele, R.B. (1994) General Structure Analysis System (GSAS). Los Alamos National Laboratory Report LAUR 86-748.
Lind, M.D. and Housley, R.M. (1972) Crystallization studies of lunar igneous rocks: crystal structure of synthetic armalcolite. Science, 175, 521–523.
Lindsley, D.H., Kesson, S.E., Hartzman, M.J., and Cushman, M.K. (1974) The stability of armalcolite: Experimental studies in the system MgO-Fe-Ti-O. Proceedings of the 5th Lunar Science Conference, Geochimica et Cosmochimica Acta, Supplement 5, 1, 521–534.
Moore, C.H., Jr. and Sigurdson, H. (1949) Petrology of high titanium slags. Transactions of the American Institution of Mining and Metallurgical Engineers, 185, 914–919.
Navrotsky, A. (1975) Thermodynamics of formation of some compounds with the pseudobrookite structure and of the $FeTi_2O_5$-Ti_3O_5 solid solution series. American Mineralogist, 60, 249–256.
Navrotsky, A. and Kleppa, O.J. (1967) The thermodynamics of cation distributions in simple spinels. Journal of Inorganic and Nuclear Chemistry, 29, 2701–2714
Oganov, A.R. and Brodholt, J.P. (2000) High-pressure phases in the Al_2SiO_5 system and the problem of aluminous phase in the Earth's lower mantle: ab initio calculations. Physics and Chemistry of Minerals, 27, 430–439.
Onoda, M. (1998) Phase transitions of Ti_3O_5. Journal of Solid State Chemistry, 136, 67–73.
Pauling, L. (1930) The crystal structure of pseudobrookite. Zeitschrift für Kristallographie, 73, 97–112.
Pownceby, M.I. and Fisher-White, M.J. (1999) Phase equilbria in the systems Fe_2O_3-MgO-TiO_2 and FeO-MgO-TiO_2 between 1173 and 1473 K, and Fe^{2+}-Mg mixing properties of ilmenite, ferrous-pseudobrookite and ulvöspinel solid solutions. Contributions to Mineralogy and Petrology, 135, 198–211.
Redfern, S.A.T., Henderson, C.M.B., Wood, B.J., Harrison, R.J., and Knight, K.S. (1996) Determination of olivine cooling rates from metal-cation ordering. Nature, 381, 407–409.
Redfern, S.A.T., Harrison, R.J., O'Neill H.St.C., and Wood, D.R.R. (1999) Thermodynamics and kinetics of cation ordering in $MgAl_2O_4$ spinel up to 1600 °C from in situ neutron diffraction. American Mineralogist, 84, 299–310.
Robinson, K., Gibbs, G.V., and Ribbe, P.H. (1971) Quadratic elongation—quantitative measure of distortion in coordination polyhdera. Science, 172, 567–570.
Smith, R.I., Hull, S., and Armstrong, A.R. (1994) The POLARIS Powder Diffractometer at ISIS. Proceedings of the Third European Powder Diffraction Conference (EPDIC-3), Vienna, Austria, 1993. Materials Science Forum, 251–256, 166–169.
Sugiyama, K. and Takéuchi, Y. (1991) The crystal-structure of rutile as a function of temperature up to 1600 °C. Zeitschrift für Kristallographie, 194, 305–313.
Swanson, D.K. and Peterson, R.C. (1980) Polyhedral volume calculations. Canadian Mineralogist, 18, 153–156.
Thompson, J.B. Jr. (1969) Chemical reactions in crystals. American Mineralogist, 54, 341–375.
Waldbaum, D.R. (1973) The configurational entropies of $Ca_2MgSi_2O_7$-$Ca_2SiAl_2O_7$ melilites and related minerals. Contributions to Mineralogy and Petrology, 39, 33–54.
Wechsler, B.A. (1977) Cation distribution and high-temperature crystal chemistry of armalcolite. American Mineralogist, 62, 913–920.
Wechsler, B.A. and Navrotsky, A. (1984) Thermodynamics and structural chemistry of compounds in the system MgO-TiO_2. Journal of Solid State Chemistry, 55, 165–180.
Wechsler, B.A. and Von Dreele, R.B. (1989) Structure refinements of Mg_2TiO_4, $MgTiO_3$ and $MgTi_2O_5$ by time-of-flight neutron powder diffraction. Acta Crystallographica, B45, 542–549.
Xirouchakis, D., Smirnov, A., Woody, K., Lindsley, D.H., and Andersen, D.J. (2002) Thermodynamics and stability of pseudobrookite-type $MgTi_2O_5$ (karrooite). American Mineralogist, 87, 658–667.
Yang, H. and Hazen, R.M. (1998) Crystal chemistry of cation order-disorder in pseudobrookite-type $MgTi_2O_5$. Journal of Solid State Chemistry, 138, 238–244.
——— (1999) Comparative high-pressure crystal chemistry of karrooite, $MgTi_2O_5$, with different ordering states. American Mineralogist, 84, 130–137.

Manuscript received May 24, 2006
Manuscript accepted January 24, 2007
Manuscript handled by Przemyslaw Dera